EUROPEAN ORGANIZATION FOR NUCLEAR RESEARCH

CERN/EP 81-18
13 March 1981

INCLUSIVE ρ^0, $K^{*\pm}(892)$ AND f PRODUCTION IN $\bar{p}p$ INTERACTIONS AT 12 GeV/c

V. Karimäki*, R. Kinnunen*, M. Korkea-aho and J. Tuominiemi*
Department of High Energy Physics, University of Helsinki, Helsinki

G.W. van Apeldoorn, D. Harting, D.J. Holthuizen and B.J. Pijlgroms*
NIKHEF-H/Zeeman Laboratorium, Amsterdam**

P.J. Johnson, P. Mason, P. Michaelides***, Ch. Michaelidou+, H. Muirhead* and G.D. Patel
Department of Physics, University of Liverpool, Liverpool

G. Ekspong, T. Moa and S. Nilsson
Institute of Physics, University of Stockholm, Stockholm

Submitted to Zeitschrift für Physik C

---

* Present address: CERN, Geneva, Switzerland

** Part of the joint research program of FOM and ZWO

*** Permanent address: Department of Nuclear Physics University of Athens

\+ Permanent address: Department of Physics University of Crete

0404P/HM/mk

ABSTRACT

Inclusive production of ρ^0, $K^{*\pm}(892)$ and f is studied in $\bar{p}p$ interactions at 12 GeV/c. The inclusive cross sections for ρ^0, $K^{*\pm}(892)$ and f are found to be 6.7 ± 0.3 mb, 1.0 ± 0.2 mb and 1.4 ± 0.3 mb, respectively. The differential cross sections are presented as a function of c.m. rapidity, Feynman x and square of the transverse momentum p_T^2. Comparison with the corresponding pp data shows some interesting differences which can be attributed to the $\bar{p}p$ annihilation. The results are compared with the predictions of the quark fusion model.

1. INTRODUCTION

The inclusive study of resonance production has provided a great deal of information on the structure of hadrons and their interactions. It has become clear that a large fraction of the particles observed in the final state are produced indirectly through the decays of resonances. Furthermore, the results from the inclusive studies of resonance production have lent support to the concept of the quark-parton picture of hadrons. In order to reach a better understanding of the soft scattering phenomena it is therefore necessary to have data on reactions with a variety of quantum numbers involved.

There have been several experimental investigations on the inclusive ρ^0 and $K^{*\pm}(892)$ production in $\bar{p}p$ interactions at various energies [1-11]. In this work we present the results on the reactions

$$\bar{p}p \to \rho^0 + X \qquad (1)$$

$$\bar{p}p \to K^{*+} + X \qquad (2)$$

$$\bar{p}p \to K^{*-} + X \qquad (3)$$

$$\bar{p}p \to f + X \qquad (4)$$

at 12 GeV/c beam momentum. The annihilation component is still relatively important at this energy and we try to deduce its characteristics by comparing our data at 12 GeV/c with the pp data at the same energy.

The main features of the non-strange vector meson production can be understood in phenomenological quark models like, for instance, the quark fusion model [12-14], which is a simple generalization of the Drell-Yan model [15] to hadron production at low energies. The prediction that the fragmentation spectrum of the produced meson is essentially given by the valence quark distribution functions of the incident hadron is also a feature the quark recombination model [16]. A characteristic of the quark fusion mechanism is the possibility of the interaction of valence quarks, which may be of considerable importance in low energy $\bar{p}p$ collisions. The model has been shown to give a reasonable description for the vector meson data in pp interactions [12]. In $\pi^{\pm}p$ and $K^{\pm}p$ interactions [12-13] the model has shown to give a fairly good description of the shapes of the vector meson spectra.

This paper is arranged as follows: a short description of the experimental procedure will be given in sect. 2; the total inclusive and semi-inclusive cross sections are given in sect. 3; the transverse and longitudinal momentum distributions are presented and compared with the corresponding pp data in sect. 4; in sect. 5 the results are discussed in terms of the simple quark fusion model and finally, our conclusions are summarized in sect. 6.

2. EXPERIMENTAL PROCEDURE

The present work is based on the data obtained from an exposure of the CERN 2 m hydrogen bubble chamber to a 12 GeV/c antiproton beam. The results of the ρ^0 and f production are based on a sample of 83 054 inelastic events obtained in this experiment. In the study of $K^{*\pm}(892)$ production a sample of 11 312 events with visible V^0 decay has been used.

The tracks measured in all inelastic events were passed through a mass dependent Hydra geometry program. For momenta below about 1.5 GeV/c the ionization on the track was used to reject wrong mass hypotheses. In ambiguous cases all mass hypotheses that gave a fit were included in the sample with the corresponding weight factor.

The ρ^0 and f mesons are detected through the decay processes

$$\rho^0,\ f \to \pi^+\pi^- \tag{5}$$

and K^{*+} and K^{*-} through the decay processes

$$K^{*\pm} \to K_s^0 \pi^{\pm} \tag{6}$$

where the neutral kaon is identified by its decay into π^+ and π^-.

The data have been corrected for the K_s^0 decays outside the fiducial volume and for those too close to the vertex to be detectable. More details of the experimental procedure are given in ref. [7].

The distribution of the $\pi^+\pi^-$ invariant mass for all inelastic events is shown in fig. 1. A ρ^0 enhancement is seen upon the background. The f signal is not easily visible in this plot but can be better seen in fig. 2, which presents the distribution of the $\pi^+\pi^-$ invariant mass multiplied by the factor exp (2.5 $m_{\pi^+\pi^-}$/GeV). The procedure of multiplying by an exponential in mass enhances the structure in the high mass region and compensates for the sharply falling background below the f mass.

A small shoulder can be seen below the ρ^0 enhancement in fig. 1. This structure was observed to shift the mass of ρ^0 to significantly smaller values in the fits than given in the PDG tables [17]. A detailed investigation indicated that the shoulder is a reflection of the $K^{*0}(892)$ resonance due to unresolved $\pi^\pm/K^\pm$ ambiguities. We took all possible $\pi^\pm K^\pm$ combinations and changed in these the kaon mass into the pion mass. The $\pi^+\pi^-$ mass distribution thus obtained was observed to peak at 680 MeV for combinations with the $K\pi$ mass in the $K^{*0}(892)$ band, whereas for combinations with the $K\pi$ mass outside this band no peak was seen in the faked $\pi^+\pi^-$ mass distribution. Because of the relative smallness of the $K^*(892)$ signal a quantitative estimate of its contribution is, however, impossible.

The effective mass spectrum for the $K_s^0\pi^+$ and $K_s^0\pi^-$ combinations is presented in fig. 3. For simplicity, we have here taken all charged tracks to be pions, which means that the $K_s^0\pi^\pm$ mass spectrum is contaminated by $K_s^0 p$ and $K_s^0\bar{p}$ combinations. This procedure does not, however, influence the K^* signal since the wrong combinations are spread relatively uniformly in the background distribution. We have checked this by using the ionization information for the tracks with momentum less than 1.5 GeV/c. The shape of the mass distribution did not change.

A clear resonance signal can be seen in the effective mass spectrum at the position of $K^*(892)$. We do not observe any evidence for the production of $K^*(1420)$. Therefore in the following K^* always refers to $K^*(892)$. Some structure can also be seen in the distribution below the $K^*(892)$ mass region. A possible explanation for this is an influx of

wrongly identified Λ^0's taken as K^0's. We have checked that this is not the case by selecting a sample of unambiguous K^0_s's with appropriate cuts in the decay angle of the negative decay track in the V^0 rest frame. The structure does not disappear and therefore we take it to be a statistical fluctuation.

We have described the $\pi^+\pi^-$ and $K^0_s\pi^\pm$ mass distributions with the general function

$$\frac{d\sigma}{dm} = \alpha BG + \beta BG \cdot BW \qquad (7)$$

where α and β are parameters to be determined, BG is the background function and BW the relativistic Breit-Wigner form

$$BW(m) = \frac{m\, m_R\, \Gamma(m)}{(m^2-m_R^2)^2 + m_R^2\, \Gamma^2(m)} \quad . \qquad (8)$$

In eq. (8)

$$\Gamma(m) = \Gamma_R (q/q_R)^{2\ell+1} m_R/m \qquad (9)$$

where m_R is the mass and Γ_R the width of the resonance, q is the momentum of one of the decay products in the resonance rest frame, q_R is the momentum at the resonance mass and ℓ is the angular momentum of the resonance.

The fits were carried out over the following mass intervals;

from 0.6 GeV to 1.0 GeV in the case of ρ^0,
from 1.0 GeV to 1.5 GeV in the case of f and
from 0.64 GeV to 1.22 GeV in the case of $K^{*\pm}(892)$.

In the fits the PDG table values [17] were used for the mass and the width of the resonance. In this work the formula

$$BG = Ae^{-Bm+Cm^2} \qquad (10)$$

was found to fit satisfactorily the form of the background for the $\pi^+\pi^-$ mass. More complicated parametrisations do not improve the

confidence level of the fits. The parameter C was not found to be significantly different from zero. In the $K^0\pi^{\pm}$ mass distribution (fig. 3) the K^*-region is still influenced by the threshold behaviour i.e. by the rapid increase of the spectrum to its maximum value just below the K^* mass. We have therefore chosen for the background the following parametrization

$$BG = a(m-m_T)^b \, e^{-cm-dm^2} \qquad (11)$$

where m_T is the threshold mass.

Extending the fits for ρ^0 and f beyond the given regions leads to poorer fits due to the rapid change of the background. This indicates that the exponential behaviour of the background (10) is valid only in a narrow region of the mass spectrum.

The differential cross section in a given variable was obtained by dividing the data into intervals in this variable and fitting the expression (7) as described above to the appropriate mass spectrum in each such interval. To increase the statistics we have folded data from the CP symmetric combinations $K_s^0\pi^-$ and $K_s^0\pi^+$ to determine the distributions of the K^{*+}.

3. INCLUSIVE AND SEMI-INCLUSIVE CROSS SECTIONS

The inclusive cross sections for the production of ρ^0, $K^{*\pm}(892)$ and f were found to be

$$\sigma(\rho^0) = 6.7 \pm 0.3 \text{ mb}$$
$$\sigma(K^{*\pm}) = \sigma(K^{*+}) + \sigma(K^*) = 1.0 \pm 0.2 \text{ mb}$$
$$\sigma(f) = 1.4 \pm 0.3 \text{ mb}.$$

The above values include the corrections for the unseen decay modes of $K^{*\pm}$ and f. The quoted error includes the statistical error, the

systematic error due to the choice of the parametrization of the background and the uncertainty in the absolute normalization. The fits were satisfactory with the χ^2/ND values varying around one in most cases.

The results of the fits are shown in figs 1, 2 and 3. As can be seen from the fitted curve in fig. 1 the reflection of $K^{*0}(892)$ does not contribute to the ρ^0 cross section when the mass is not allowed to vary.

The ρ^0 cross section in another, smaller statistics experiment at 12 GeV/c [2], is in good agreement with our cross section. We have also determined the inclusive cross section $\sigma(K^{*\pm})$ in our earlier paper [7] with a different kind of background function, determined from experimental data. The value obtained in ref. [7] is 0.95 ± 0.1 mb, which agrees well with the present value within the limits of the estimated systematic error. Our value is also in good agreement with the K^* cross section determined in the 12 GeV/c $\bar{p}p$ BEBC experiment [10].

Using the results on the production of charged pions and K_s^0's in our experiment [7] it was found that about 10% of all charged pions are decay products of ρ^0 and about 23% of the produced K_s^0 mesons come from the decay of $K^{*\pm}$ resonances at this energy.

Comparison of our results with the cross sections measured in pp interactions for the production of ρ^0, K^{*+} and K^{*-}, 1.80 ± 0.25 mb, 0.27 ± 0.03 mb and $0.04\ ^{+0.02}_{-0.03}$ mb [18] respectively, would suggest that about 70% of the ρ^0 and $K^{*\pm}$ resonances in $\bar{p}p$ interactions at 12 GeV/c are produced in annihilation reactions.

The inclusive cross section of ρ^0 in $\bar{p}p$ [1-6], pp [19-21] and $\pi^{\pm}p$ [22] interactions at different beam momenta are shown in fig. 4. In $\bar{p}p$ interactions the inclusive cross section increases logarithmically at high energies and seems to obtain its minimum around the beam momentum of 12 GeV/c. Fig. 5 shows the inclusive cross section of $K^{*\pm}$ in $\bar{p}p$ interactions [7-11] and that of K^{*+} in pp interactions [18, 20, 23] as a function of beam laboratory momentum. The cross section for $K^{*\pm}$ in $\bar{p}p$ reactions is seen to decrease with increasing momentum in the low energy range. This is clearly a consequence of the rapid decrease of the

annihilation component which dominates particle production in $\bar{p}p$ interactions at low energies. It is expected that at high energies the $K^{*\pm}$ cross section will have the same behaviour as the K^{*+} cross section in pp interactions, as seen in fig. 5.

Table 1 shows the ρ^0 cross section for different charge multiplicities. A considerable amount of ρ^0's are produced with the six prong topology. The average number of ρ^0's per inelastic event, $<\rho^0>$, and the ratios of ρ^0's to positive pions, $<\rho^0>/<\pi^+>$, given in the table, increase with the increasing multiplicity. The increase of $<\rho^0>/<\pi^+>$ seems to be characteristic for $\bar{p}p$ interactions [4] and might be explained with the abundant ρ^0 production in the annihilation processes, which are expected to dominate at high multiplicities.

Table 2 shows the f cross sections with decay into two charged pions $<f>$ and $<f>/<\pi^+>$ for different charge multiplicities. Again a significant increase in the average numbers of f's and in the ratios of f's to positive pions with increasing multiplicity can be observed.

The topological cross sections for the production of $K^{*\pm}$ are given in table 3. A sizable portion of the $K^{*\pm}$ are seen to be produced in the four and six-prong topology. The average number of the produced $K^{*\pm}$ per inelastic collision, shown also in the table, seems to increase with increasing charged multiplicity.

4. DIFFERENTIAL CROSS SECTIONS

The distributions in p_T^2, the square of the transverse momentum, for ρ^0, $K^{*\pm}$ and f are shown in figs 6, 7 and 8, respectively. The cross sections are seen to fall approximately exponentially with increasing p_T^2. Thus the function

$$\frac{d\sigma}{dp_T^2} = A \exp(-B\, p_T^2)$$

has been fitted to the experimental distributions. The resulting slope parameters and the range of p_T^2 in each fit are shown in table 4. The values are consistent with those obtained in other $\bar{p}p$ experiments at low energies [1-6, 8-11].

The behaviour of the p_T^2 distributions for ρ^0 and K^{*+} in pp interactions [19,18] are also shown in figs 6 and 7. No significant difference in slopes, which could be attributed to the $\bar{p}p$ annihilation, can be seen between the $\bar{p}p$ and pp data.

For comparison we also show in fig. 7 the p_T^2 distribution for K_s^0 as obtained in this experiment [7]. The distribution decreases rapidly in the small p_T^2 range, $p_T^2 \lesssim 0.5$ (GeV/c)^2, as a consequence of the K_s^0 meson production through the decay of resonances, mainly K^* [24].

The distributions for ρ^0, K^{*+} and f in the c.m. rapidity are presented in figs 9, 10 and 11 and those in the x variable for ρ^0 and K^{*+} in figs 12 and 13.

The distributions for ρ^0 and f are characterized by broad maxima in the central region, suggesting a dominantly central production. In fig. 14 the rapidity distribution of ρ^0 is compared with the 22.4 [4] and 100 [1] GeV/c data. The available rapidity range is seen to increase but the production in the central region remains essentially constant between 12 and 100 GeV/c.

From figs 10 and 13 it can be seen that the K^{*+} is produced mainly in the proton fragmentation region although the cross section in the antiproton fragmentation region is also fairly large.

In fig. 15 we compare the c.m. rapidity distribution, obtained by adding the K^{*+} and K^{*-} distributions(*), with the data on the

---

(*) The K^{*-} distribution is just the CP reflection of the K^{*+} distribution in fig. 13.

production of K^{*+} in pp interactions at 12 GeV/c [18]. In pp interactions the cross section for K^{*-} at 12 GeV/c has been measured to be very small, $0.04\ ^{+0.02}_{-0.03}$ mb [18]. Addition of the K^{*-} contribution to the pp spectrum would give a small increase in the region $y^* \sim 0$. The dashed curve in this figure represents the difference of the $\bar{p}p$ and pp data.

The cross section of $K^{*\pm}$ in $\bar{p}p$ interactions is much larger than in pp collisions. This may be explained by double K^* production, which should be strong in $\bar{p}p$ interactions because of the valence antiquarks present in the initial state. Namely, production of a $K^{*+}(K^{*+} = u\bar{s})$ and $K^{*-}(K^{*-} = \bar{u}s)$ simultaneously requires only one $s\bar{s}$ pair from the sea, whereas in pp interactions a $u\bar{u}$ pair also should be created to produce the K^{*+} K^{*-} pair.

Furthermore it can be seen from fig. 15 that the spectrum in $\bar{p}p$ reactions is broader than that in pp interactions. In the former case the K^*'s are produced with a larger average longitudinal momenta as can be seen from the difference of the y^* distributions. The ratio of the K^* distributions in $\bar{p}p$ and pp interactions, shown as a function of $|y^*|$ in fig. 16, increases with increasing rapidity.

The difference between the $\bar{p}p$ and pp data must be mainly a consequence of the $\bar{p}p$ annihilation. To study this we present in fig. 17 the reflected x distribution of the $K^{*\pm}$ obtained in this analysis, that of the K^{*+} in pp interactions at 12 GeV/c [18] and the distribution obtained by extrapolation of the data on $K^{*\pm}$ production measured at 3.6 GeV/c [9] where the annihilation component is dominating. In the extrapolation of the data from 3.6 GeV/c to 12 GeV/c we have assumed that the cross section of the annihilation component decreases as $1/\sqrt{s}$ (= 0.6) with increasing energy. It is seen from the figure that the distribution obtained by summing up the pp data and the extrapolated annihilation data reproduces fairly well the spectrum of the $K^{*\pm}$ in $\bar{p}p$ interactions.

5. COMPARISON WITH THE QUARK FUSION MODEL

In the quark fusion model a meson M with a quark content $q_1\bar{q}_2$ is produced in the inclusive reaction

$$A + B \to M + \text{anything} \tag{12}$$

through the fusion of $q_1(\bar{q}_2)$ from particle A and with a $\bar{q}_2(q_1)$ from particle B. The quarks q_1 and q_2 are valence or sea quarks. In the model the cross section for the reaction (12) is proportional to the distribution functions of the appropriate quarks inside the colliding hadrons and is given by [13]

$$(x^2 + 4m_T^2/s)^{1/2}\, d\sigma/dx = d\sigma/dy^* =$$

$$(2J+1)\,\frac{1}{3}\,G_{eff}\,\frac{4\pi^2}{m_T^2}\,x_1x_2(f^A_{q_1}(x_1)f^B_{\bar{q}_2}(x_2) + f^A_{\bar{q}_2}(x_1)\,f^B_{q_1}(x_2)) \tag{13}$$

where m_M is the mass of the meson M, $y^* = \ln((p_L + E)/m_T)$ and $x = 2p_L^*/\sqrt{s} = x_1 - x_2$ are the c.m. rapidity and the reduced c.m. longitudinal momentum of the meson M and $m_T = (m_M^2 + \langle p_T^2\rangle)^{1/2}$. The parameter G_{eff} is the effective coupling constant, J is the spin of the produced meson and the factor 1/3 results from the average over the quark colours. A detailed description of the model can be found, for instance, in ref. [12-13].

The reduced longitudinal momenta x_1 and x_2 of the quarks in the fusion process have the following approximate expressions in terms of the c.m. rapidity and Feynman x of the produced meson

$$x_{1,2} = \frac{m_T}{\sqrt{s}}\,e^{\pm y^*} = \frac{1}{2}\,(\sqrt{x^2 + 4\,m_T^2/s} \pm x) \tag{14}$$

We use in our calculations the values of $\langle p_T^2\rangle$ given in sect. 4 for the ρ^0 and f, respectively. The parameter $G_{eff} = 0.5$ has been determined from the requirement of the simultaneous description of data on ρ^0 yields in πp and pp interactions [12].

The functions $f_q^i(x)$ can be expressed as a sum of the distribution functions for the valence and sea quarks

$$f_q^i(x) = V_q^i(x) + S_q^i(x) \ . \qquad (15)$$

In this work the following parametrizations for the quark distribution functions are used [25]

$$\begin{aligned} V_u^p(x) &= 1.79\ (1+2.3\ x)\ (1-x)^3/\sqrt{x} \\ V_d^p(x) &= 1.1\ (1-x)^{3.1}/\sqrt{x} \qquad (16) \\ S^p_{u,\bar{u}}(x) &= S^p_{d,\bar{d}}(x) = S^p_{s,\bar{s}}(x)/\lambda_s = 0.36\ (1-x)^7/x. \end{aligned}$$

Here λ_s is the suppression factor for the strange quarks in the sea which has been determined experimentally. The comparison of the strange and nonstrange vector meson production in pp interactions leads to $\lambda_s = 0.15$ at 12 GeV/c [18].

The x distributions of ρ^0 and K^{*+} in pp interactions at 12 GeV/c, as calculated from the model, are shown in fig. 18 compared with the experimental data [18-19]. It is seen that good agreement with the experimental spectra is obtained, except at $x = 0$.

The calculated rapidity distribution of ρ^0 in $\bar{p}p$ interactions at 12 GeV/c is presented in fig. 9 compared with the experimental data. The distributions from different types of subprocesses are also shown in the figure. The main contribution to the cross section is seen to be given by the valence-valence interaction although the fragmentation processes are also important. The valence-valence term is given by the fusion of a valence antiquark from the antiproton with a valence quark from the proton. This term is large over a wide kinematical region. The fragmentation processes are described by the valence-sea terms, which originate from the fusion of a valence quark from the proton with an antiquark from the antiproton sea (proton fragmentation) or from the fusion of a valence antiquark from the antiproton with a quark from the proton sea (antiproton fragmentation). The sea-sea term, which is given by the fusion of a quark and an antiquark from the sea of the incident particles, respectively, is very small at the energy of 12 GeV/c.

We assume that in the quark fusion approach the f meson is produced with the same mechanism as the ρ^0. Hence we have neglected all dynamical effects due to the higher spin state which are difficult to be included at a simple phenomenological level. The model predicts for f the production characteristics observed experimentally as can be seen from the curves in fig. 11.

The contributions of different mechanisms to the ρ^0 production in $\bar{p}p$ interactions as given by the model are presented in fig. 19 as a function of beam momentum. The valence-valence term, which as the difference between the $\bar{p}p$ and pp interactions represents as a first approximation the annihilation processes, is seen to dominate at low energies. It has the asymptotic behaviour $\ln s/\sqrt{s}$. The increase with energy below 50 GeV/c must be partly due to kinematic threshold effects but may also indicate failure of the asymptotic assumptions of the model at low energies. The valence-sea term seems to approach a constant limit at high energies thus explaining the scaling behaviour of the fragmentation spectra. The production from the sea quarks is neglible at small energies but dominates at very high energies. The behaviour of the different components as a function of energy can explain the form of the rapidity distributions of ρ^0 in fig. 14. The decrease of the interaction of valence quarks and the increase of the sea quark fusion leads to an approximately constant cross section in the central region between 12 and 100 GeV/c. The rise in the total cross section is mainly due to the increase of the fragmentation components. In pp interactions, on the contrary, one expects a continuous rise in the ρ^0 cross section also in the central region.

Fig. 20 shows the energy behaviour of the summed total inclusive cross section of ρ^0 in $\bar{p}p$ interactions as compared with the experimental data [1-6]. The calculated cross section is in agreement with the experimental numbers above 12 GeV/c. As was concluded above, the model cannot be expected to give the cross section reliably at low energies and it is also not obvious at which beam momentum the comparison with data becomes meaningful. The agreement at 12 GeV/c may hence still be fortuitous. The calculated inclusive cross section of f as a function of beam momentum, also shown in fig. 20, increases more slowly than that of ρ^0 due to the

kinematical effect of the larger mass of f meson. The energy dependence of the ρ^0 cross section in pp interactions compared with the experimental data [18-19] is shown for comparison.

The prediction of the model for the production of $K^{*\pm}$ is exactly the same for $\bar{p}p$ and pp interactions. This means that the experimental distributions of $K^{*\pm}$ in pp and $\bar{p}p$ collisions cannot be simultaneously described. The difference in the ρ^0 production between the $\bar{p}p$ and pp interactions is provided in the model by the fusion of the valence quarks of the proton with the valence antiquarks of the antiproton. In the case of K^*, however, the production through valence-valence fusion is not possible in $\bar{p}p$ interactions.

One possible explanation for the peripheral nature of the annihilation process in $\bar{p}p$ interactions would be that the valence quarks which are going to annihilate are very slow ($x \approx 0$) and consequently the valence quarks left over are correspondingly faster ($x \approx 1$). We have therefore made an attempt to describe the shape of the annihilation component of the $K^{*\pm}$ spectrum by parametrizing the valence quark distribution functions of the proton in such a way as to account for the large average longitudinal momentum of the K^*.

The annihilation cross section for K^{*+} would then be given by the fusion of the extremely fast ($x \approx 1$) valence u quark of the proton with a $\bar{s}$ from the sea of the antiproton for the K^{*+} and similarly for K^{*-} by the fusion of the fast ($x \approx 1$) $\bar{u}$ quark of the antiproton with an s quark from the sea of the proton. For the fast valence quark we have used the form given by the Kuti-Weisskopf model [26]

$$V_u^p(x) = 2V_d^p(x) = 2\,\frac{\Gamma(\gamma+3[1-\alpha(0)])}{\Gamma(1-\alpha(0))\,\Gamma(\gamma+2[1-\alpha(0)])}\,x^{-\alpha(0)}(1-x)^{-1+\gamma+2[1-\alpha(0)]} \qquad (17)$$

where γ and $\alpha(0)$ are parameters to be determined from the data. For the determination of these parameters we use the data on $K^{*+}(892)$ production in $\bar{p}p$ interactions at 3.6 GeV/c, where the non-annihilation component is found to be small [9]. A fit of the valence-sea term in

eq. (13) to the x distribution of $K^{*+}(892)$ at 3.6 GeV/c [27] extrapolated to 12 GeV/c yields the following parameter values

$$\gamma = 0.50 \pm 0.03$$

$$\alpha(0) = 0.17 \pm 0.04.$$

We have performed the fit over the range $x < -0.5$, because here the behaviour of the incident valence quark should be clearly visible. Using the extended model which includes the annihilation component as described above we have calculated the prediction for the c.m. rapidity distribution of K^{*+}. The results are compared with the experimental data in fig. 10. The partial distributions from the VS, SS and the annihilation terms are also shown in the figure. Although better agreement in the proton fragmentation region is now obtained than without the modification the disagreement in the forward hemisphere still remains. This would suggest that the characteristic features of the annihilation component are not as simply reproduced as is described above. It seems presumable, for instance, that the strange quarks which can be created in the annihilation of the valence quark-antiquark pairs also contribute to the K^* production.

6. CONCLUSIONS

The production of ρ^0, K^{*+}, K^{*-} and f in $\bar{p}p$ interactions has been studied and compared with the corresponding pp data. The results have been discussed in terms of the simple quark fusion model. The results can be summarized as follows.

The inclusive cross section for the production of ρ^0, $K^{*\pm}$ and f in $\bar{p}p$ interactions at 12 GeV/c are found to be 6.7 ± 0.4 mb, 1.0 ± 0.2 mb and 1.4 ± 0.3 mb, respectively. Comparison with the corresponding pp data suggest that ρ^0 and $K^{*\pm}$ are abundantly produced in the $\bar{p}p$ annihilation.

The p_T^2 distributions fall exponentially with increasing p_T^2 with the slopes around 3 $(GeV/c)^{-2}$ and ρ^0 and $K^{*\pm}$ and around 2 $(GeV/c)^{-2}$ for f.

The ρ^0 and the f are observed to be produced centrally. The K^{*+} is produced dominantly in the proton fragmentation region although significant production occurs also in the forward hemisphere. Comparison of the c.m. rapidity distribution for $K^{*\pm}$ with the corresponding pp data shows that in $\bar{p}p$ interactions the K^{*+} and K^{*-} are produced with larger average longitudinal momenta than in pp reactions. The difference between the $\bar{p}p$ and pp spectra can be reproduced by the low energy data on $\bar{p}p$ annihilation as extrapolated to the present energy.

The longitudinal distributions of ρ^0 and f can be described in the quark fusion model. Also the interesting feature of the approximately constant cross section in the central region in the energy range 12 to 100 GeV/c can be explained by the different energy dependence of the valence-valence and sea-sea quark interactions in the model. However, the model fails to describe the large ρ^0 and f inclusive cross sections in $\bar{p}p$ interactions below 10 GeV/c beam momentum.

It was also observed that the production of K^{*+} in pp interactions can be reasonably well described in the quark fusion model. However, the model does not provide any difference between the K^* production in pp and $\bar{p}p$ interactions and thus fails to reproduce correctly the cross section and distributions of the K^* in the latter case. Especially, the larger average longitudinal momentum remains unexplained. We have tried to modify the model by describing the annihilation component separately with different distribution functions for the valence quarks. We assumed that the valence quarks which annihilate are slow and therefore the u quark responsible for the formation of the $K^{*\pm}$ is fast. The experimental results on the $K^{*\pm}$ production in $\bar{p}p$ interactions at 3.6 GeV/c were used to parametrize the distribution of the fast ($x \approx 1$) valence quark. The two component model was, however, observed to be unable to give a complete explanation for the features shown by the experimental K^{*+} spectrum in $\bar{p}p$ interactions at 12 GeV/c.

Acknowledgements

Two of us (P.J. Johnson and G.D. Patel) and the groups of Helsinki and Stockholm wish to thank their National Science Research Councils for support during the course of this work.

REFERENES

[1] R. Raja et al., Phys. Rev. D16 (1977) 2733

[2] D. Gall et al., Particle and resonance production in $\bar{p}p$ interactions, at 12 GeV/c, Proc. Int. Symp. on pp Interactions, Loma-Koli, Finland, June 1975

[3] P.S. Gregory et al., Nucl. Phys. B119 (1977) 60

[4] D.I. Ermilova et al., Nucl. Phys. B137 (1978) 29

[5] C.K. Chen et al., Phys. Rev. D17 (1978) 17

[6] M. Markytan et al., Nucl. Phys. B143 (1978) 263

[7] P. Johnson et al., General features of the $\bar{p}p$ interactions at 12 GeV/c, Nucl. Phys. B173 (1980) 77

[8] A.M. Cooper et al., Nucl. Phys. B136 (1978) 365

[9] S. Banerjee et al., Z. Physik C. Particles and Fields 3, (1979) 1-8

[10] J.F. Baland et al., Nucl. Phys. B140 (1978) 220

[11] J. Canter et al., Phys. Rev. D20 (1979) 1029

[12] V.V. Kniazev et al., Hadron production of mesons in parton model, Preprint IHEP 77-106 (1977), Serpukhov

[13] P.V. Chliapnikov et al., Nucl. Phys. B148 (1979) 400

[14] S. Nandi, V. Rittenberg and H. Schneider, Phys. Rev. D17 (1978) 1336

[15] S.D. Drell and T.M. Yan, Phys. Rev. Lett. 25 (1970) 316

[16] L. van Hove and S. Pokorski, Nucl. Phys. B86 (1975) 243
K.P. Das and R.C. Hwa, Phys. Lett. 68B (1977) 459

[17] Particle Data Group, Review of particle properties, Phys. Lett. 75B (1978) 1

[18] K. Böckmann et al., Nucl. Phys. B166 (1980) 278

[19] V. Blobel et al., Phys. Lett. 48B (1974) 73

[20] V.V. Ammosov et al., Incl. production of ρ^0 and K^* resonances in pp interactions at 69 GeV/c, Saclay preprint DphPE 75-08 M-19

REFERENCES (Cont'd)

[21] R. Singer et al., Phys. Lett. 60B (1976) 385
A. Susuki et al., KEK preprint 78-13A
M.G. Albrow et al., Nucl. Phys. B155 (1979) 39

[22] B. Haber et al., Phys. Rev. D11 (1975) 495
T. Kitagaki et al., paper submitted to the XVI Inter. Conf. on High Energy Physics, Batavia, Illinois 1972
P. Borzalta et al., Nuovo Cimento 15A (1973) 45
J. Brau et al., Nucl. Phys. B99 (1975) 232
D. Fong et al., Phys. Lett. 60B (1975) 124
F.C. Winkelman et al., ibid. 56B (1975) 101
H.A. Gordon et al., Phys. Rev. Lett. 34 (1975) 284

[23] R. Singer et al., Nucl. Phys. B135 (1978) 265
H. Kishimi et al., Phys. Rev. D20 (1979) 37

[24] H. Kirk et al., Nucl. Phys. B128 (1977) 397

[25] R. McElhaney and S.F. Tuan, Phys. Rev. D8 (1973) 2267

[26] J. Kuti and V.F. Weisskopf, Phys. Rev. D4 (1971) 3418

[27] S. Banerjee, Private communication

TABLE CAPTIONS

Table 1 The ρ^0 cross sections, the average numbers of ρ^0's and the ratio of ρ^0's to produced positive pions for different charged multiplicities. The inclusive numbers are obtained from the fit to the total $\pi^+\pi^-$ mass distribution. Here the statistical errors only are given.

Table 2 The f cross sections for the decay made $\pi^+\pi^-$, the average numbers of f's and the ratio of f's to produced positive pions for different charged multiplicities. The inclusive numbers and errors as above.

Table 3 The inclusive $K^{*\pm}$ cross sections and average numbers of produced $K^{*\pm}$'s for different charged multiplicities. The inclusive numbers are obtained from the fit to the total inclusive $K^0_s\pi^\pm$ mass distribution. Here the statistical errors only are given.

Table 4 The results of the fit of an exponential function to the p_T^2 distributions for the reactions $\bar{p}p \to \rho^0 + X$, $\bar{p}p \to K^{*\pm} + X$ and $\bar{p}p \to f + X$.

TABLE 1

Prongs	σ(mb)	$\langle\rho^0\rangle$	$\langle\rho^0\rangle/\langle\pi^+\rangle$
2	0.34 ± 0.07	0.03 ± 0.01	0.05 ± 0.02
4	1.91 ± 0.16	0.12 ± 0.01	0.08 ± 0.01
6	2.78 ± 0.19	0.35 ± 0.02	0.14 ± 0.01
8	1.40 ± 0.14	0.58 ± 0.06	0.15 ± 0.02
10	0.30 ± 0.09	0.67 ± 0.20	0.12 ± 0.03
12	0.03 ± 0.02	0.65 ± 0.46	0.10 ± 0.07
Sum	6.76 ± 0.31	0.17 ± 0.01	0.11 ± 0.01
Inclusive	6.72 ± 0.13	0.17 ± 0.01	0.10 ± 0.004

TABLE 2

Prongs	σ(mb)	$\langle f\rangle$	$\langle f\rangle/\langle\pi^+\rangle$
2	0.09 ± 0.07	0.007 ± 0.006	0.015 ± 0.011
4	0.15 ± 0.09	0.009 ± 0.006	0.007 ± 0.004
6	0.52 ± 0.19	0.067 ± 0.024	0.026 ± 0.009
8	0.32 ± 0.11	0.133 ± 0.047	0.034 ± 0.011
10	0.28 ± 0.09	0.622 ± 0.209	0.107 ± 0.036
12	0.043 ± 0.032	0.935 ± 0.720	0.142 ± 0.105
Sum	1.40 ± 0.26	0.036 ± 0.007	0.022 ± 0.004
Inclusive	1.42 ± 0.28	0.036 ± 0.007	0.022 ± 0.004

TABLE 3

Prongs	σ(μb)	$\langle K^{*\pm} \rangle$
2	273 ± 57	0.022 ± 0.005
4	375 ± 87	0.023 ± 0.005
6	345 ± 81	0.044 ± 0.009
8	91 ± 24	0.038 ± 0.010
10	≤ 24	≤ 0.053
Sum	1.08 ± 0.13 mb	0.028 ± 0.003
Inclusive	1.03 ± 0.15 mb	0.026 ± 0.004

TABLE 4

Reaction	p_T^2 (GeV(c)^2	B(GeV/c)$^{-2}$
$\bar{p}p \to \rho^0 + X$	0.0 - 2.6	3.16 ± 0.12
$\bar{p}p \to K^{*\pm} + X$	0 - 1.2	3.21 ± 0.37
$\bar{p}p \to f + X$	0. - 2.0	2.05 ± 0.37

FIGURE CAPTIONS

Fig. 1 The distribution of the $\pi^+\pi^-$ invariant mass ($m_{\pi^+\pi^-}$) of all inelastic events. The curves correspond to a fit to a Breit-Wigner from (solid curve) plus a background (dashed curve) in the ρ^0 mass range.

Fig. 2 The $\pi^+\pi^-$ invariant mass ($m_{\pi^+\pi^-}$) distribution multiplied by the factor exp (2.5 $m_{\pi^+\pi^-}$/GeV). The curves as above in the f^0 mass range.

Fig. 3 The effective mass spectrum for the $K_s^0\pi^+$ and $K_s^0\pi^-$ combinations. The curves correspond to a fit to a Breit-Wigner form (solid curve) plus a background (dashed curve) in the mass range 0.6-1.22 GeV/c^2.

Fig. 4 Inclusive ρ^0 cross sections for $\bar{p}p$, pp and $\pi^\pm p$ interactions as a function of the beam laboratory momentum. The curves are drawn to guide the eye.

Fig. 5 The inclusive cross sections for $K^{*\pm}$ production in $\bar{p}p$ interactions and for K^{*+} production in pp interactions as a function of the beam momentum in the laboratory.

Fig. 6 The differential cross section as a function of p_T^2 for the reactions $\bar{p}p \to \rho^0 X$ and $pp \to \rho^0 X$ [18]. The result of a fit to the $\bar{p}p$ data is also shown.

Fig. 7 The distribution of the transverse momentum squared of the $K^{*\pm}$ (K^{*+} and K^{*-} data folded) in the reaction $\bar{p}p \to K^{*\pm} + X$. The straight line corresponds to a fit of an exponential in p_T^2 to the data. The bahaviour of the p_T^2 distribution in the reaction $pp \to K^{*\pm} + X$ at 12 GeV/c [13] and the p_T^2 distribution of the K_s^0 the reaction $\bar{p}p \to K_s^0 + X$ are also shown in the figure.

FIGURE CAPTIONS (Cont'd)

Fig. 8 The differential cross section as a function of p_T^2 for the reaction $\bar{p}p \to fX$.

Fig. 9 The differential cross section as a function of c.m. rapidity for the reaction $\bar{p}p \to \rho^0 X$. The curves are calculated from the quark fusion model. The partial distributions are also shown.

Fig. 10 The differential cross section as a function of c.m. rapidity for the reaction $\bar{p}p \to K^{*+} + X$. The curves are calculated from the two component quark fusion model. The partial distributions from the VS and SS terms of eq. (13) and from the annihilation term as deduced from the experimental $\bar{p}p$ annihilation are also shown in the figure.

Fig. 11 The differential cross section as a function of the c.m. rapidity for the reaction $\bar{p}p \to fX$. The curves are calculated from the quark fusion model.

Fig. 12 The differential cross section as a function of x for the reaction $\bar{p}p \to \rho^0 X$.

Fig. 13 The differential cross section as a function of x for the reaction $\bar{p}p \to K^{*+} + X$.

Fig. 14 Comparison of the c.m. rapidity distributions for ρ^0 in $\bar{p}p$ interactions at 12 GeV/c, 22.4 GeV/c [4] and 100 GeV/c [1]. Curves shown are calculated from the quark fusion model.

Fig. 15 Comparison of the c.m. rapidity distributions of the added K^{*+} and K^{*-} contributions in $\bar{p}p$ interactions and of the K^{*+} in pp interactions [18] at 12 GeV/c.

Fig. 16 The ratio of the distributions for K^{*+} in $\bar{p}p$ and pp [18] interactions at 12 GeV/c as a function of the absolute value of the c.m. rapidity.

FIGURE CAPTIONS (Cont'd)

Fig. 17 The distributions in the Feynman x for the reactions $pp \to K^{*\pm} + X$ at 12 GeV/c, $pp \to K^{*+} + X$ at 12 GeV/c [18], and for $\bar{p}p \to K^{*\pm} + X$ at 3.6 GeV/c [9] but extrapolated to 12 GeV/c (see text). The dashed curve corresponds to the sum of the pp data and the extrapolated low energy $\bar{p}p$ data.

Fig. 18 Predictions of the quark fusion model for the x distributions of ρ^0 and K^{*+} in pp interactions at 12 GeV/c compared with the experimental data [18,19].

Fig. 19 The energy dependence of the different production mechanisms in the quark fusion model for the reaction $\bar{p}p \to \rho^0 X$.

Fig. 20 The predictions of the quark fusion model for the energy dependence of the total ρ^0 cross sections in $\bar{p}p$ and pp interactions compared with the experimental data.

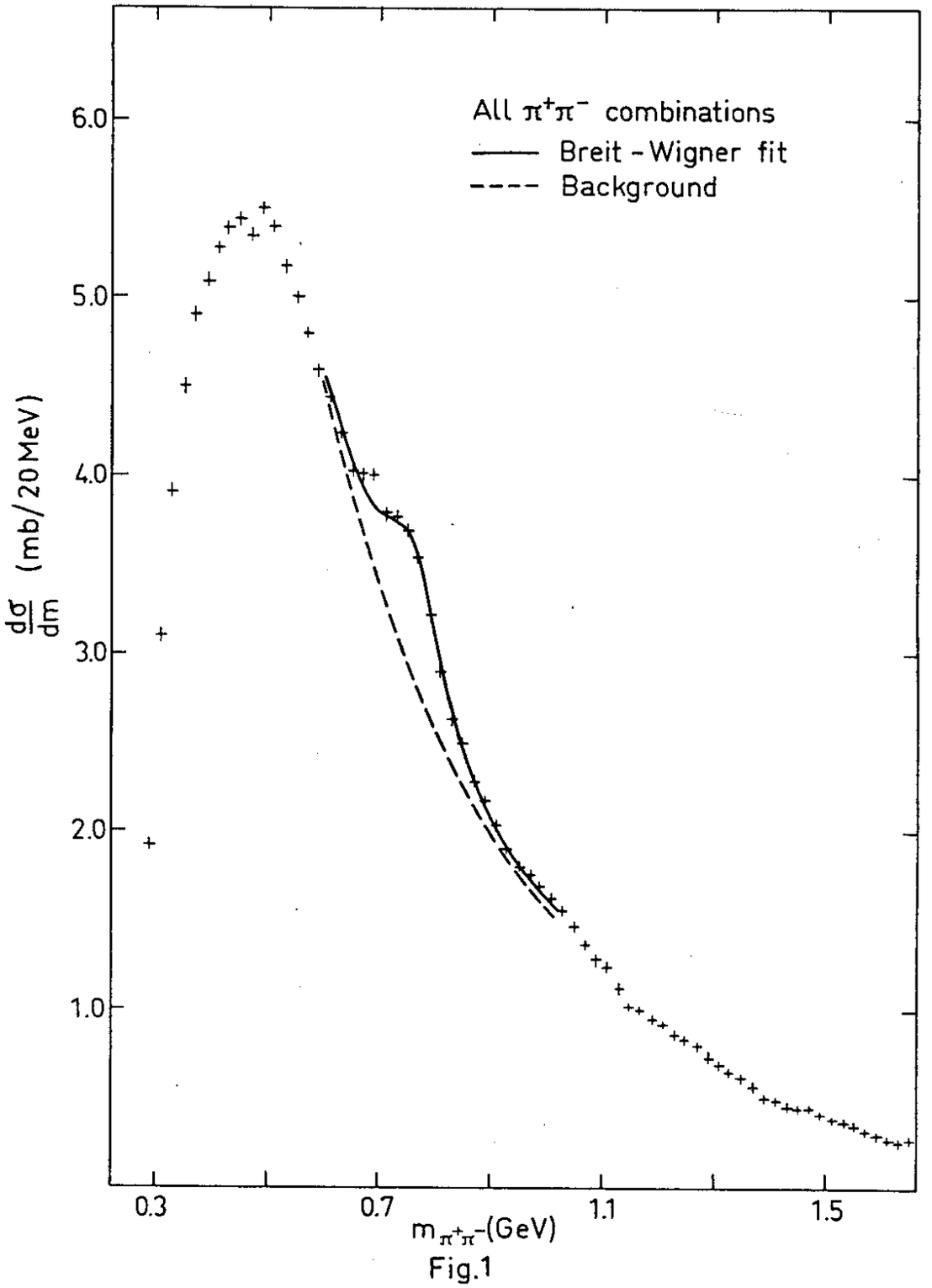
All $\pi^+\pi^-$ combinations
Breit - Wigner fit
Background
6.0
5.0
4.0
3.0
2.0
1.0
$\frac{d\sigma}{dm}$ (mb/20 MeV)
0.3
0.7
1.1
1.5
$m_{\pi^+\pi^-}$-(GeV)

Fig.1

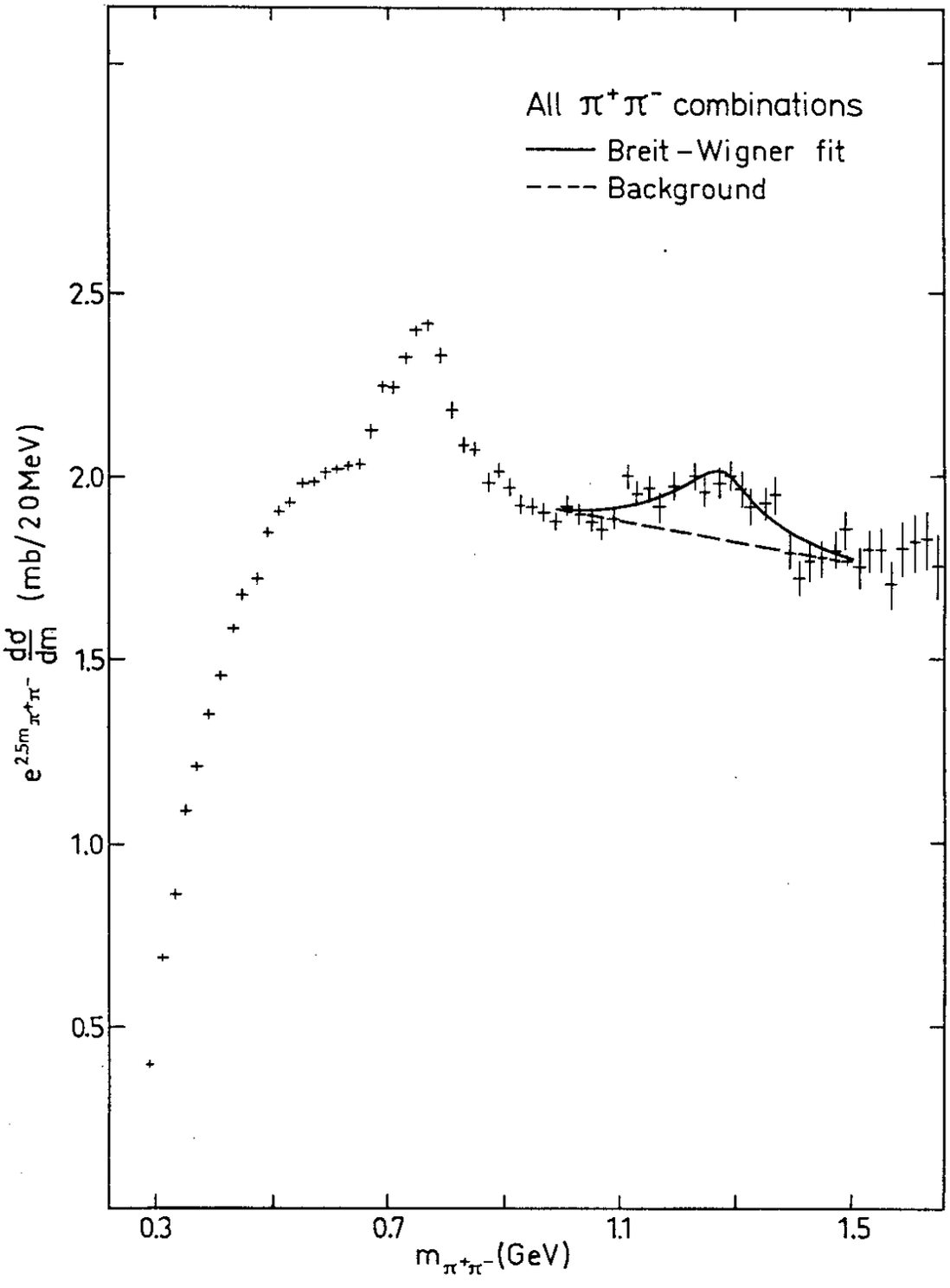
All $\pi^+\pi^-$ combinations
Breit-Wigner fit
Background
$e^{2.5m_{\pi^+\pi^-}} \frac{d\sigma}{dm}$ (mb/20MeV)
2.5
2.0
1.5
1.0
0.5
0.3
0.7
1.1
1.5
$m_{\pi^+\pi^-}$(GeV)

Fig. 2

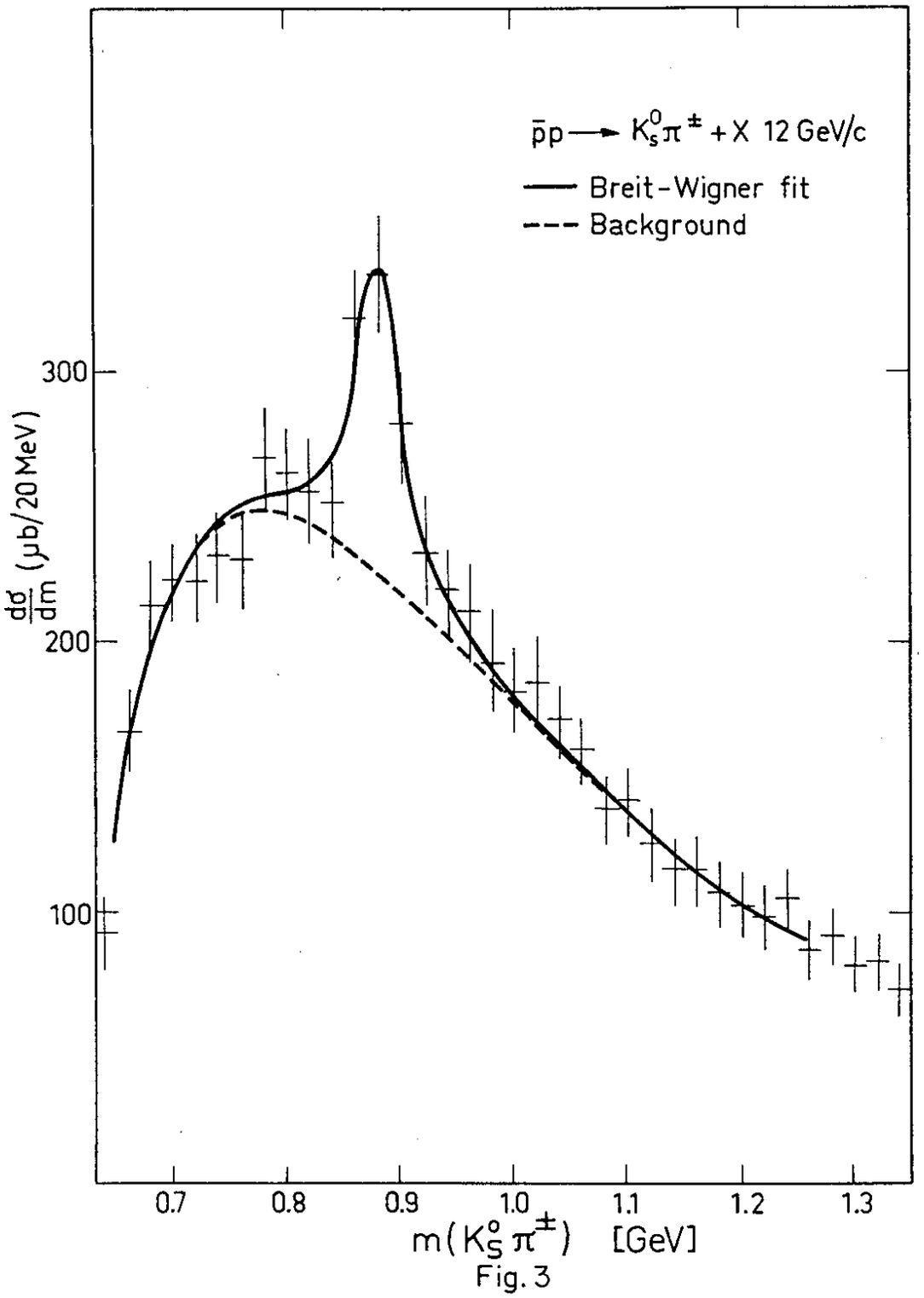
$\bar{p}p \longrightarrow K^0_s\pi^\pm + X$ 12 GeV/c
Breit-Wigner fit
Background
300
200
100
$\frac{d\sigma}{dm}$ (μb/20 MeV)
0.7
0.8
0.9
1.0
1.1
1.2
1.3
$m(K^0_S\pi^\pm)$ [GeV]

Fig. 3

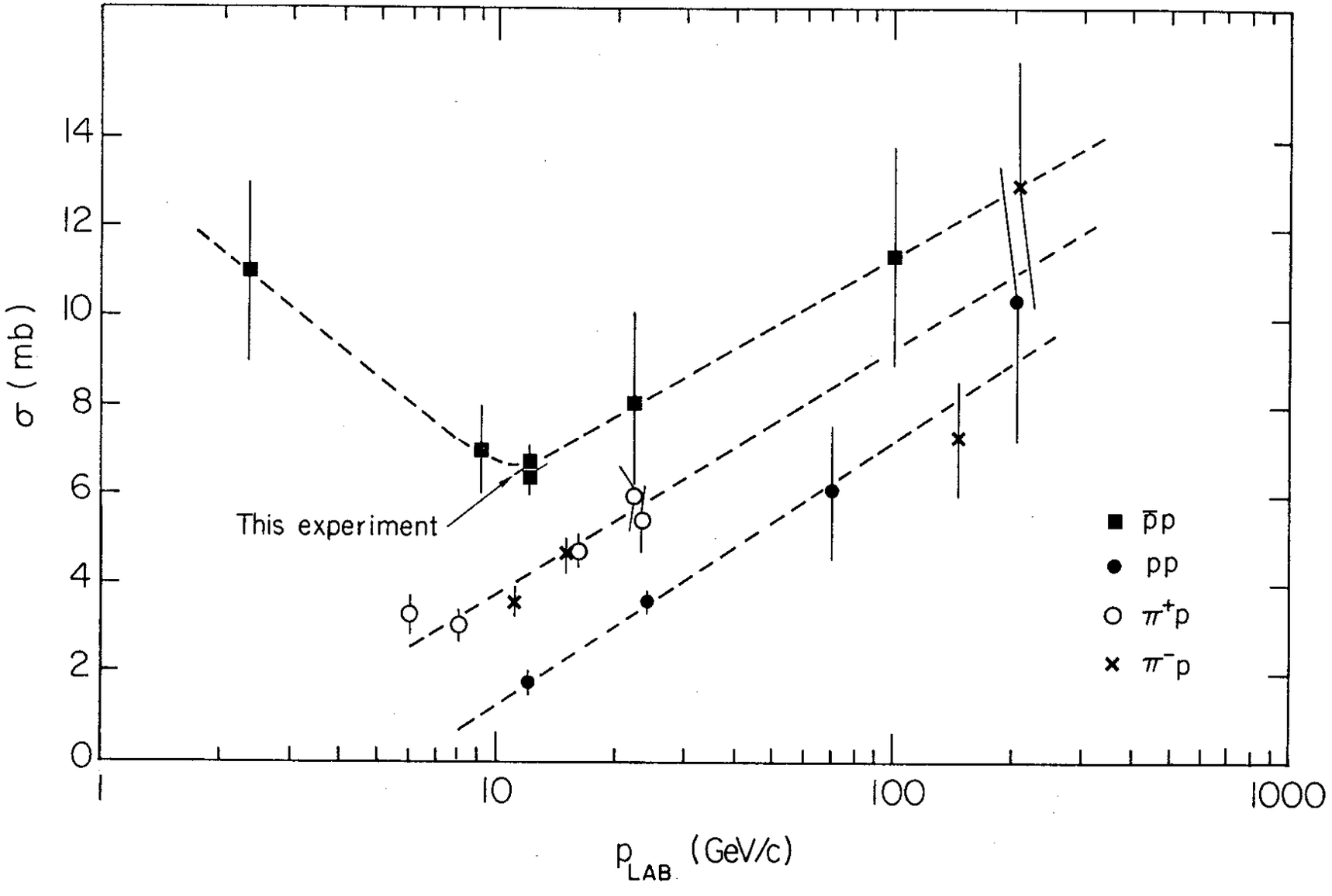
σ (mb)
0
2
4
6
8
10
12
14
1
10
100
1000
p_{LAB} (GeV/c)
This experiment
$\bar{p}p$
pp
π^+p
π^-p

Fig. 4

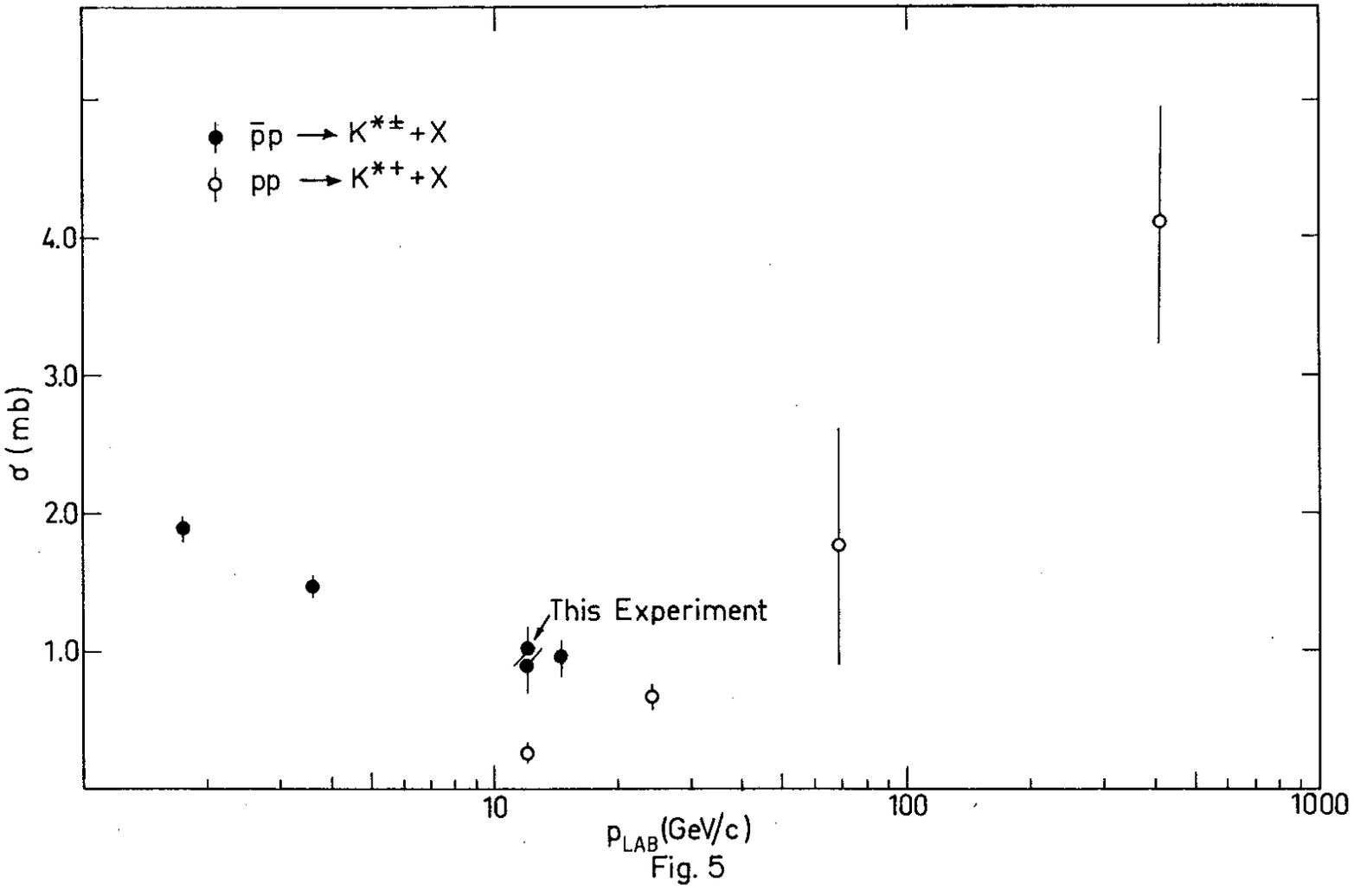
$\bar{p}p \rightarrow K^{*\pm} + X$
$pp \rightarrow K^{*+} + X$
This Experiment
σ (mb)
4.0
3.0
2.0
1.0
10
100
1000
p_{LAB}(GeV/c)
Fig. 5

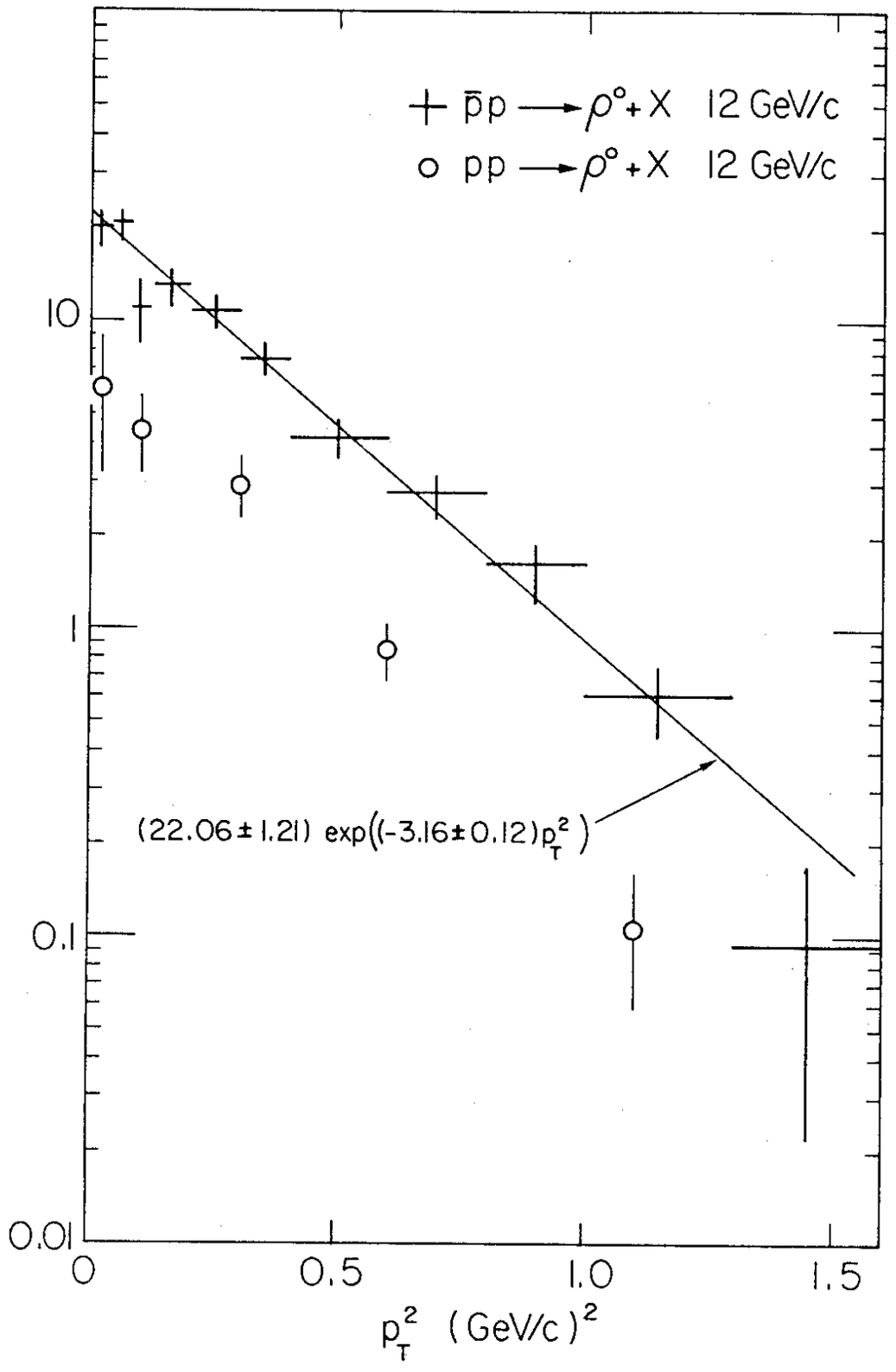
+ p̄p → ρ°+X 12 GeV/c
o pp → ρ°+X 12 GeV/c
10
1
0.1
0.01
(22.06±1.21) exp((-3.16±0.12)p_T^2)
0
0.5
1.0
1.5
p_T^2 (GeV/c)^2

Fig. 6

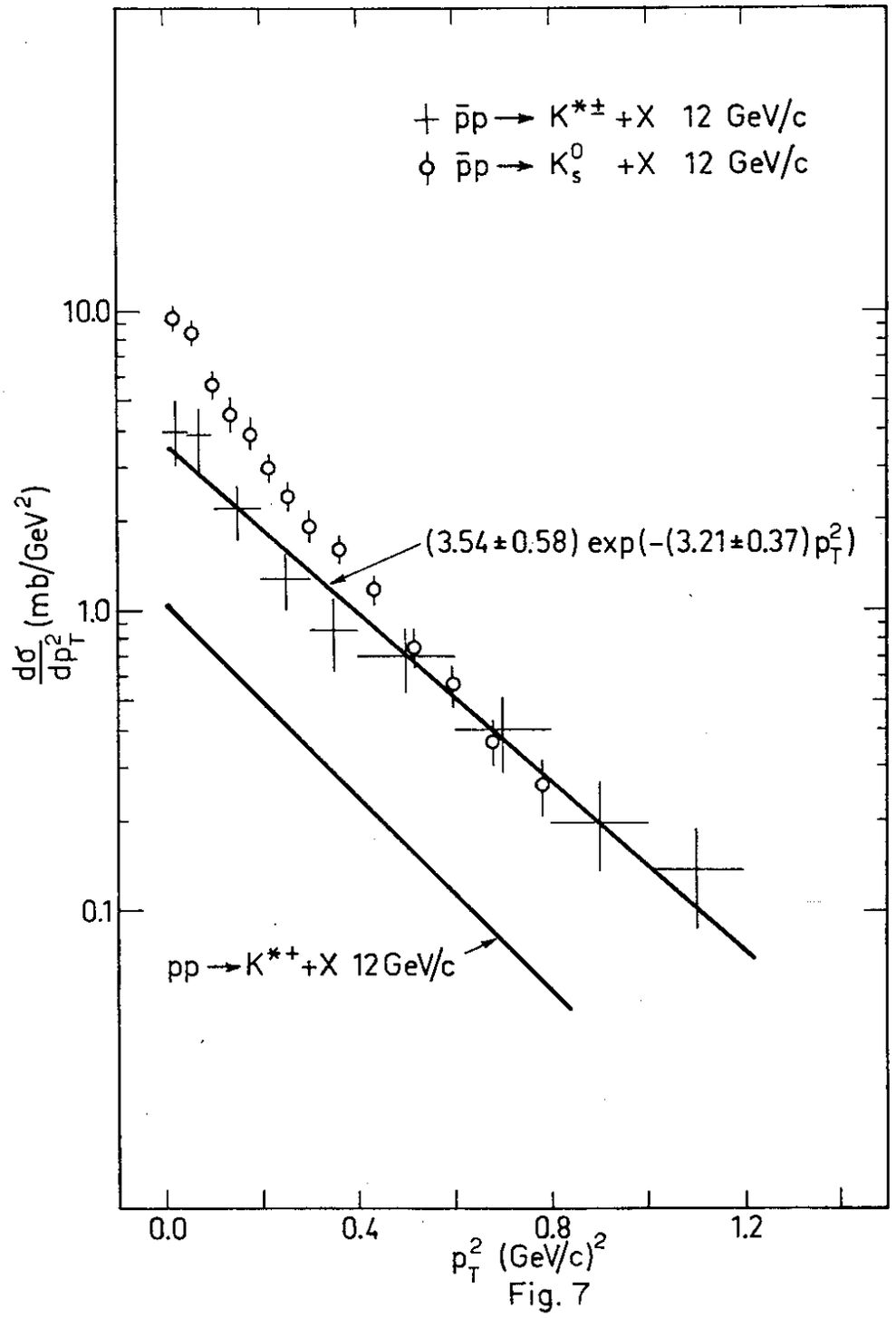
+ $\bar{p}p \rightarrow K^{*\pm} + X$ 12 GeV/c
ϕ $\bar{p}p \rightarrow K^0_s + X$ 12 GeV/c
$(3.54 \pm 0.58) \exp(-(3.21 \pm 0.37) p_T^2)$
$pp \rightarrow K^{*+} + X$ 12 GeV/c
$\frac{d\sigma}{dp_T^2}$ (mb/GeV^2)
10.0
1.0
0.1
0.0
0.4
0.8
1.2
p_T^2 (GeV/c)^2

Fig. 7

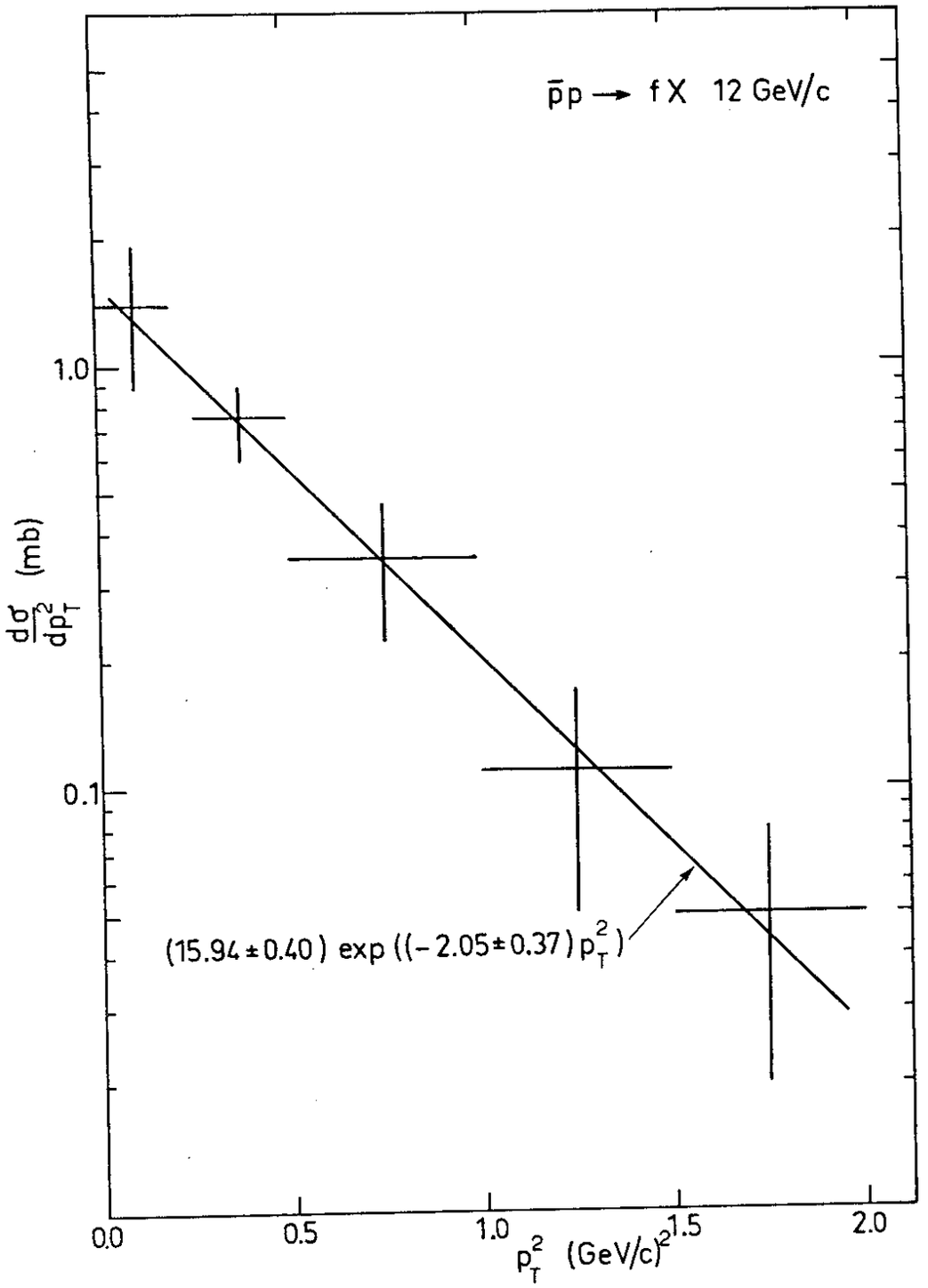
$\bar{p}p \rightarrow fX$ 12 GeV/c
1.0
0.1
$\frac{d\sigma}{dp_T^2}$ (mb)
$(15.94 \pm 0.40)\ \exp((-2.05 \pm 0.37)\, p_T^2)$
0.0
0.5
1.0
1.5
2.0
p_T^2 (GeV/c)^2

Fig.8

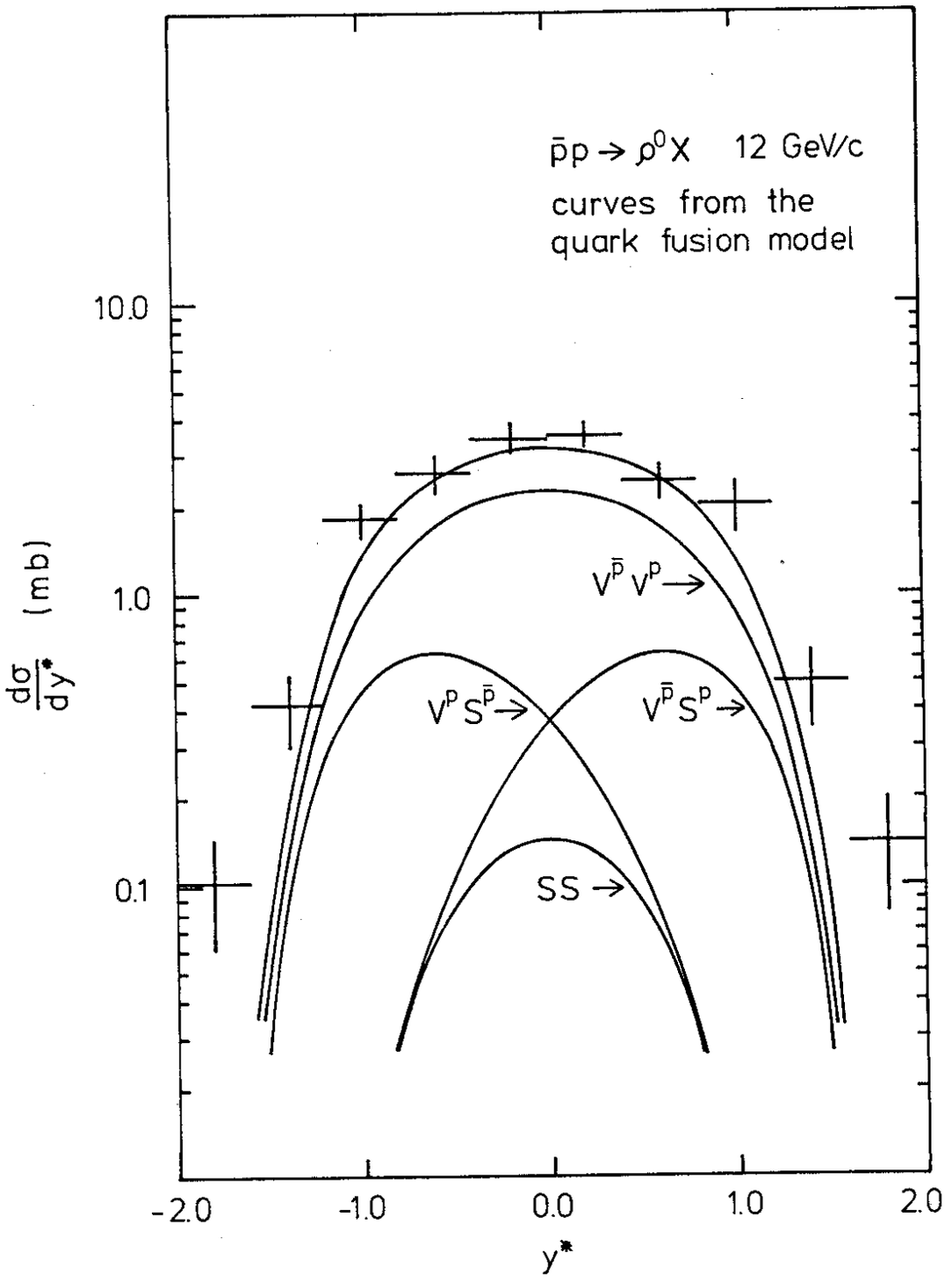
$\bar{p}p \to \rho^0 X$ 12 GeV/c
curves from the
quark fusion model
$V^{\bar{p}} V^{p} \to$
$V^{p} S^{\bar{p}} \to$
$V^{\bar{p}} S^{p} \to$
$SS \to$
10.0
1.0
0.1
$\frac{d\sigma}{dy^*}$ (mb)
-2.0
-1.0
0.0
1.0
2.0
y^*

Fig. 9

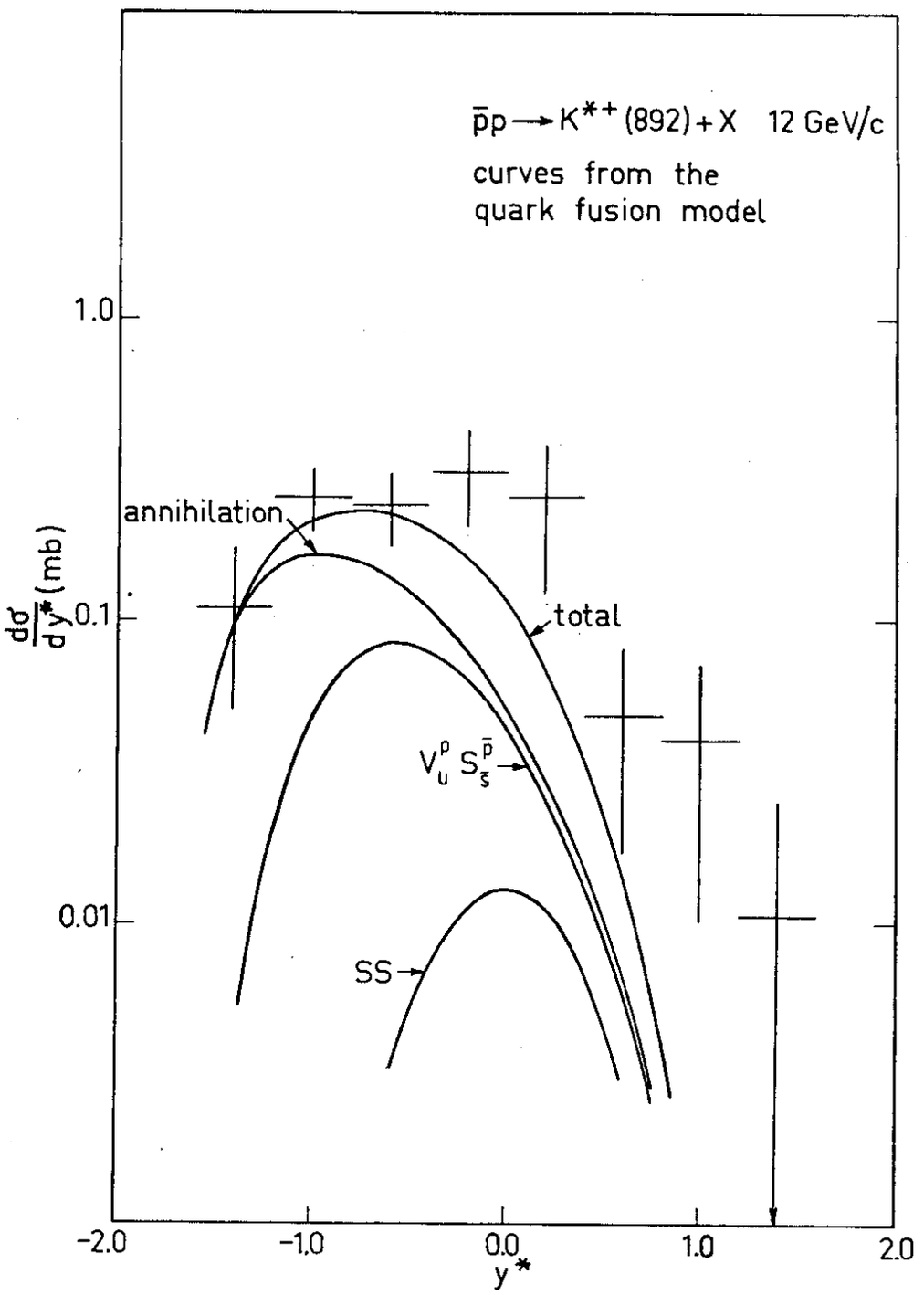
$\bar{p}p \rightarrow K^{*+}(892) + X$ 12 GeV/c
curves from the
quark fusion model
annihilation
total
$V_u^p S_{\bar{s}}^{\bar{p}}$
SS
$\frac{d\sigma}{dy^*}$ (mb)
1.0
0.1
0.01
-2.0
-1.0
0.0
1.0
2.0
y^*

Fig.10

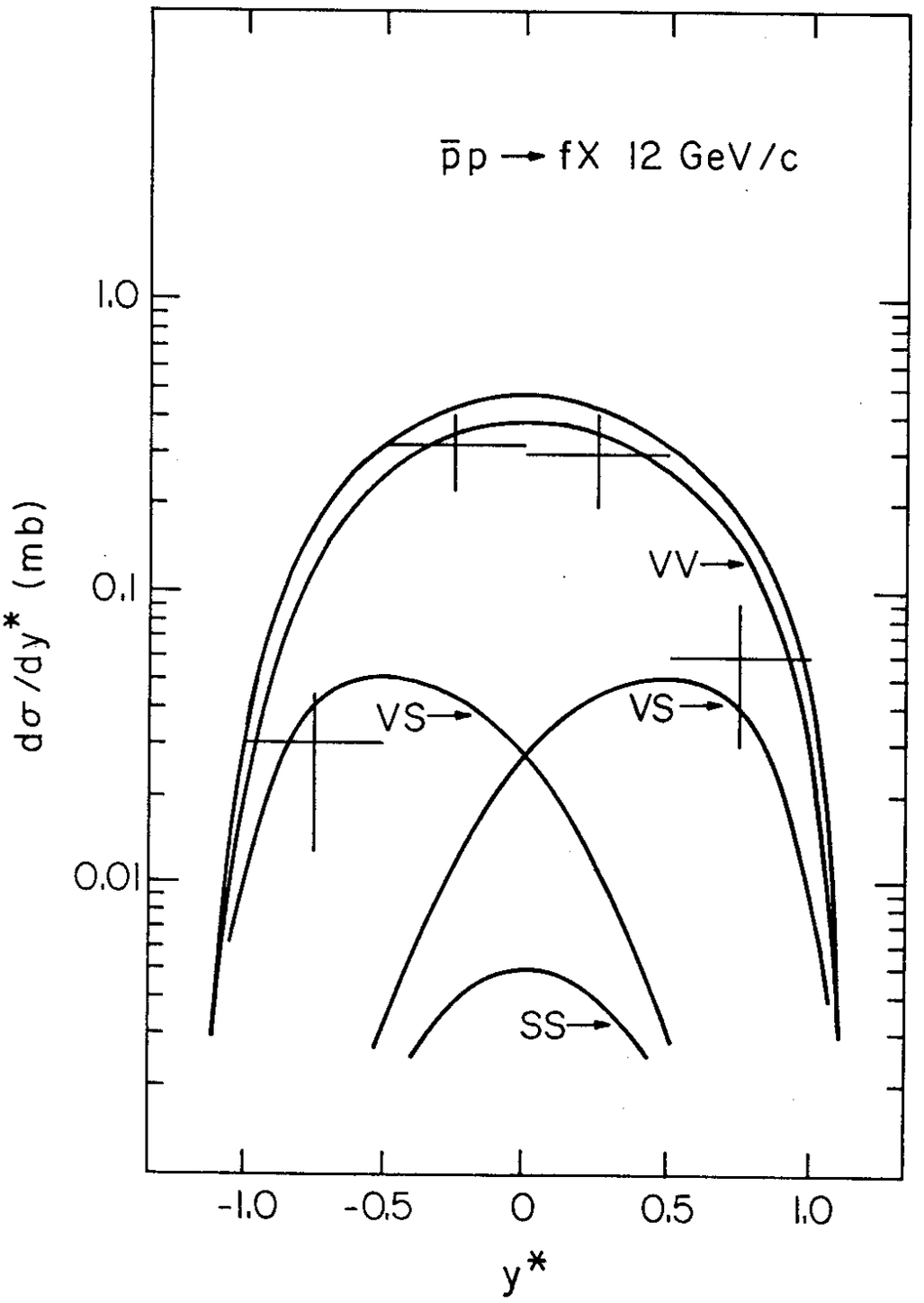
$\bar{p}p \rightarrow fX$ 12 GeV/c
1.0
0.1
0.01
$d\sigma/dy^*$ (mb)
VV
VS
VS
SS
-1.0
-0.5
0
0.5
1.0
y^*

Fig.11

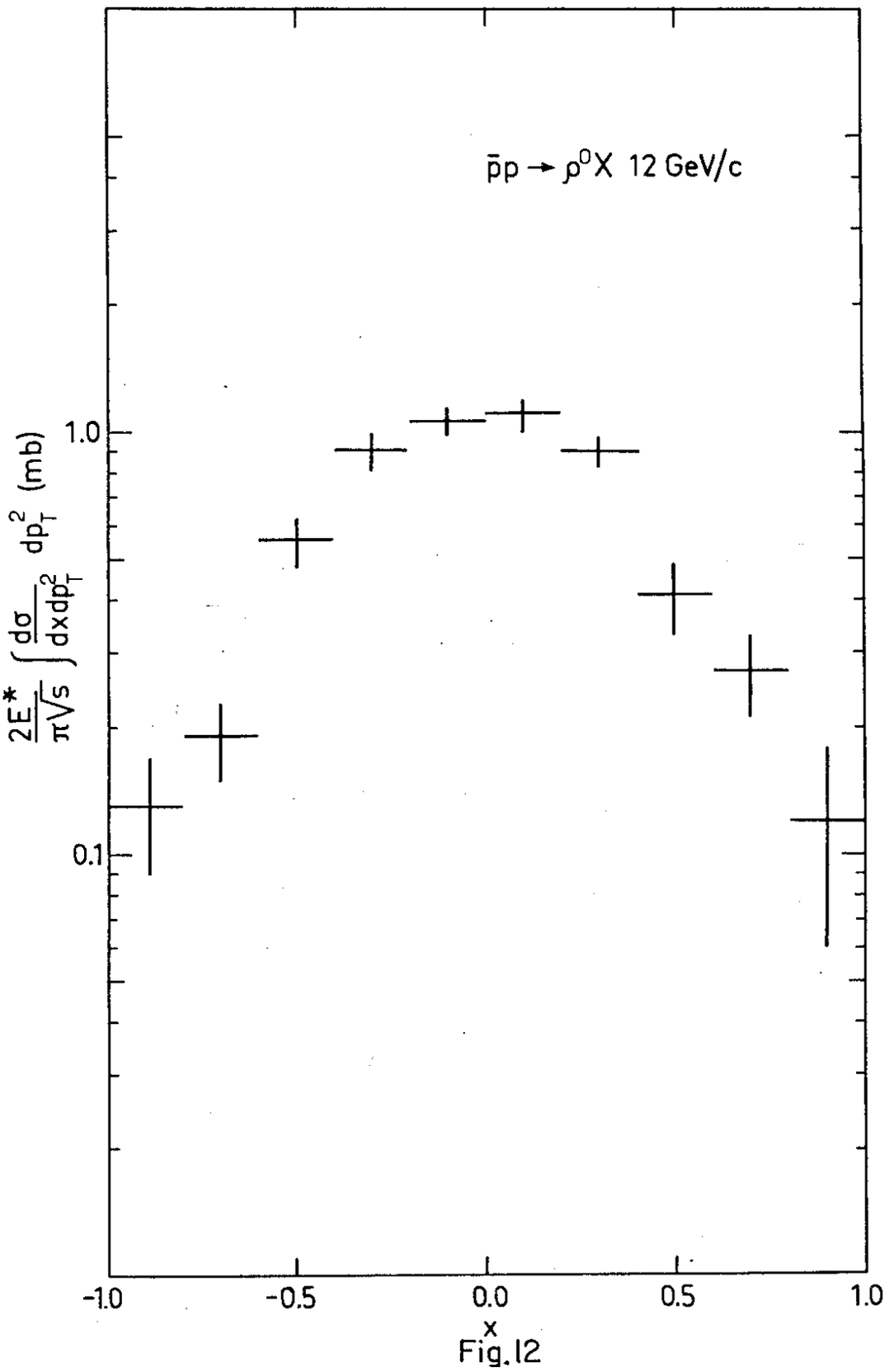
$\bar{p}p \rightarrow \rho^0 X$ 12 GeV/c
$\frac{2E^*}{\pi\sqrt{s}} \int \frac{d\sigma}{dx\,dp_T^2}\, dp_T^2$ (mb)
1.0
0.1
-1.0
-0.5
0.0
0.5
1.0
x

Fig. 12

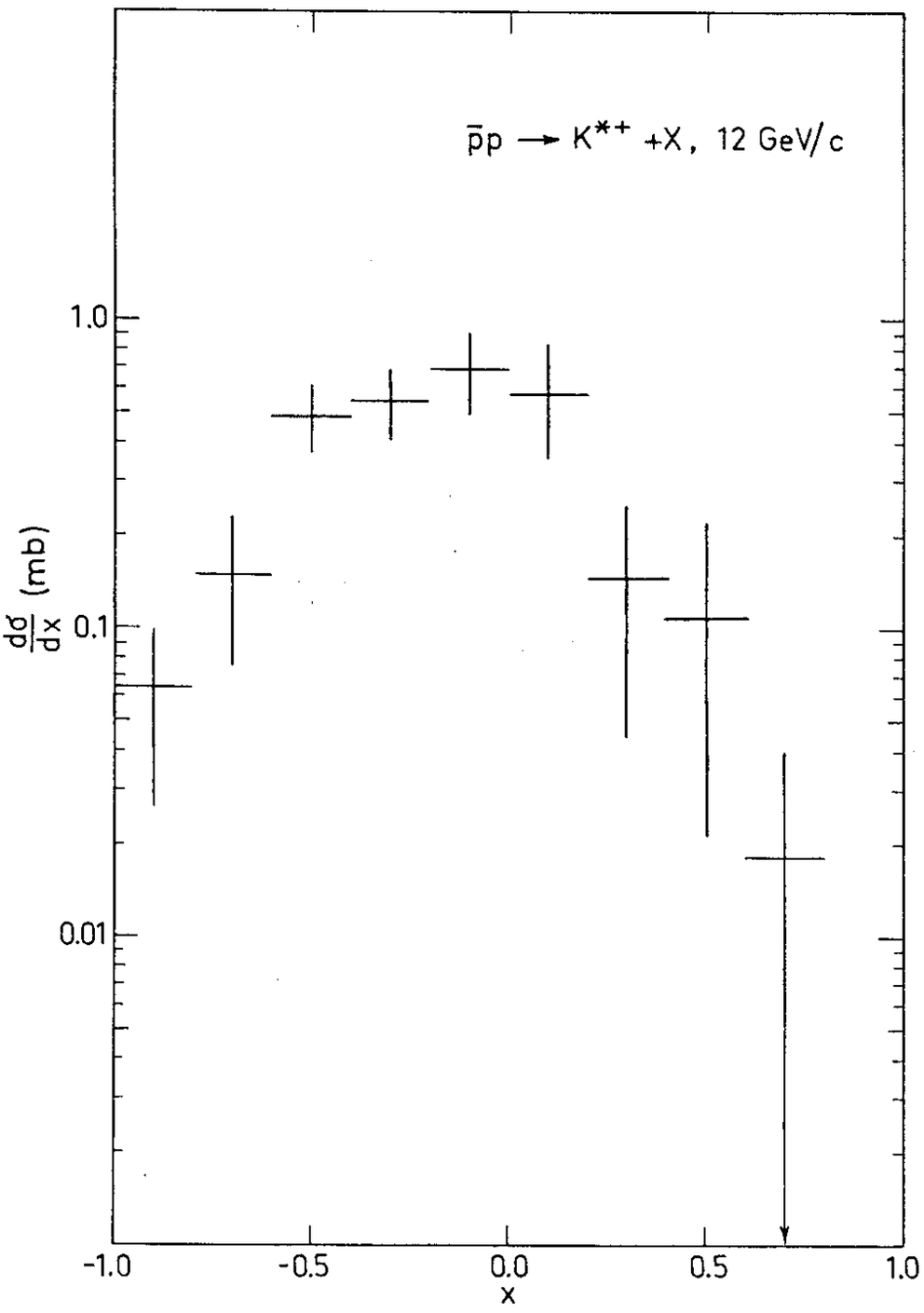
$\bar{p}p \rightarrow K^{*+} + X$, 12 GeV/c
1.0
0.1
0.01
$\frac{d\sigma}{dx}$ (mb)
-1.0
-0.5
0.0
0.5
1.0
x

Fig. 13

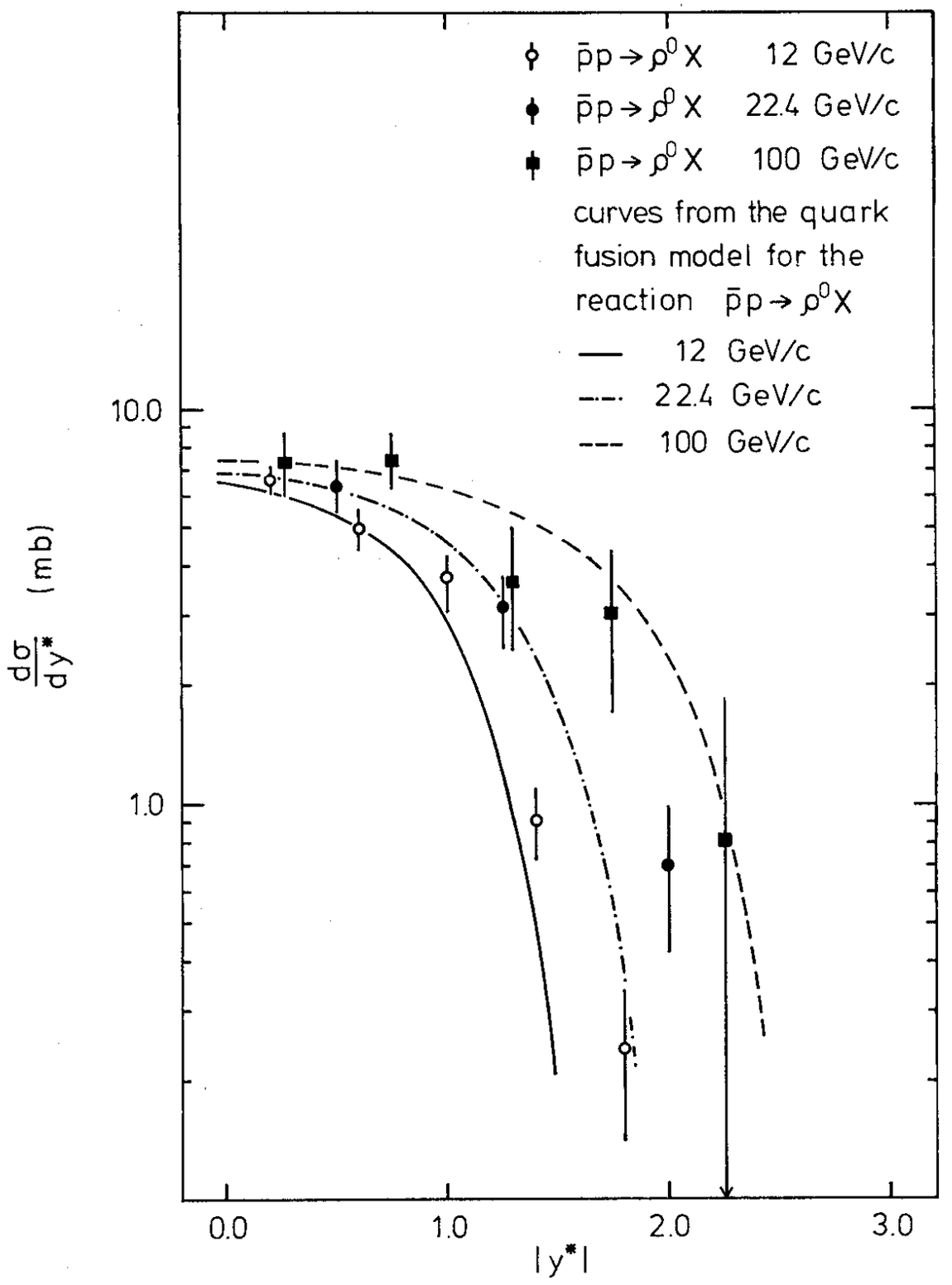
$\bar{p}p \to \rho^0 X$ 12 GeV/c
$\bar{p}p \to \rho^0 X$ 22.4 GeV/c
$\bar{p}p \to \rho^0 X$ 100 GeV/c
curves from the quark fusion model for the reaction $\bar{p}p \to \rho^0 X$
12 GeV/c
22.4 GeV/c
100 GeV/c
10.0
1.0
$\frac{d\sigma}{dy^*}$ (mb)
0.0
1.0
2.0
3.0
$|y^*|$

Fig. 14

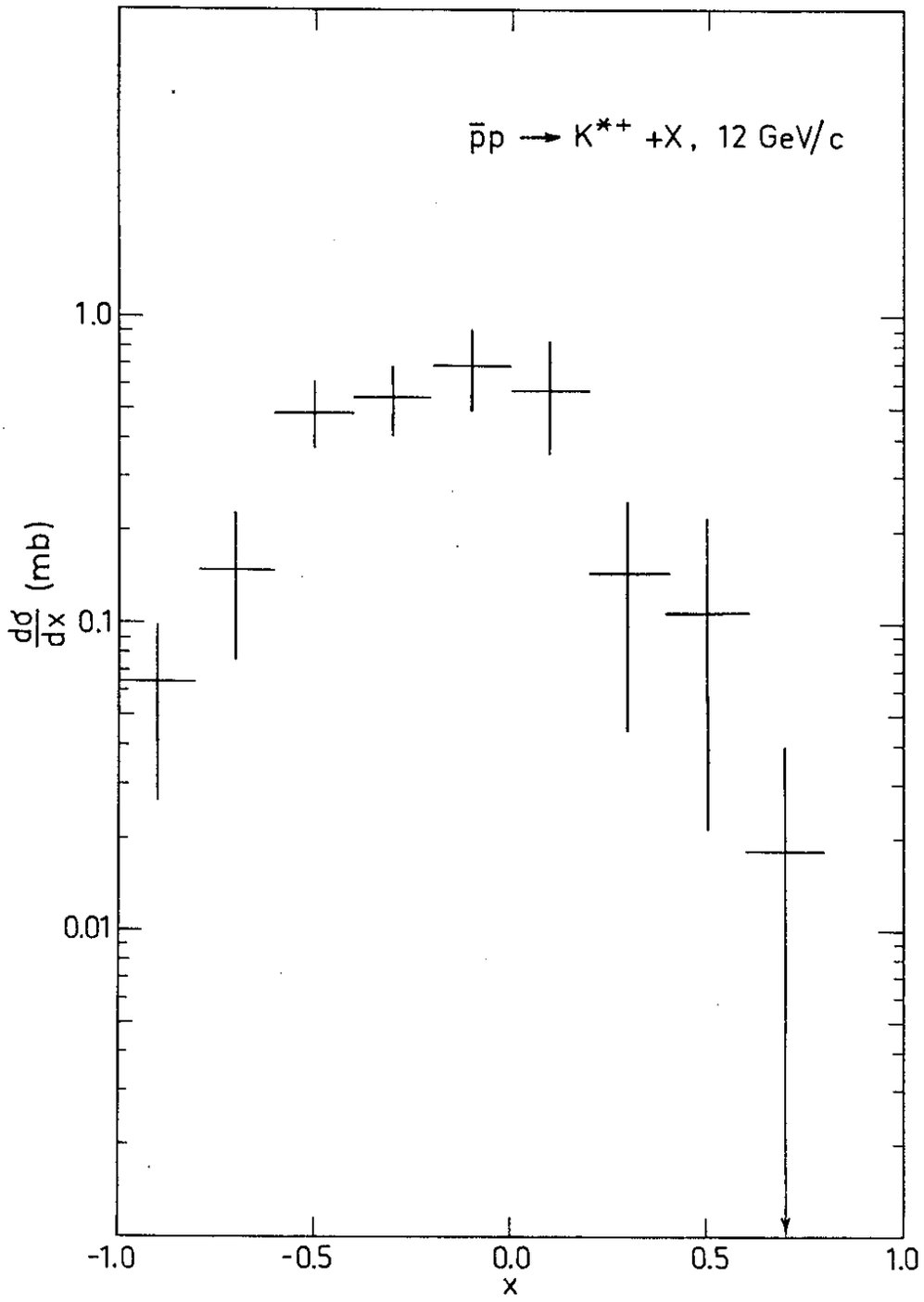
$\bar{p}p \rightarrow K^{*+} + X$, 12 GeV/c
1.0
0.1
0.01
$\frac{d\sigma}{dx}$ (mb)
-1.0
-0.5
0.0
0.5
1.0
x

Fig. 13

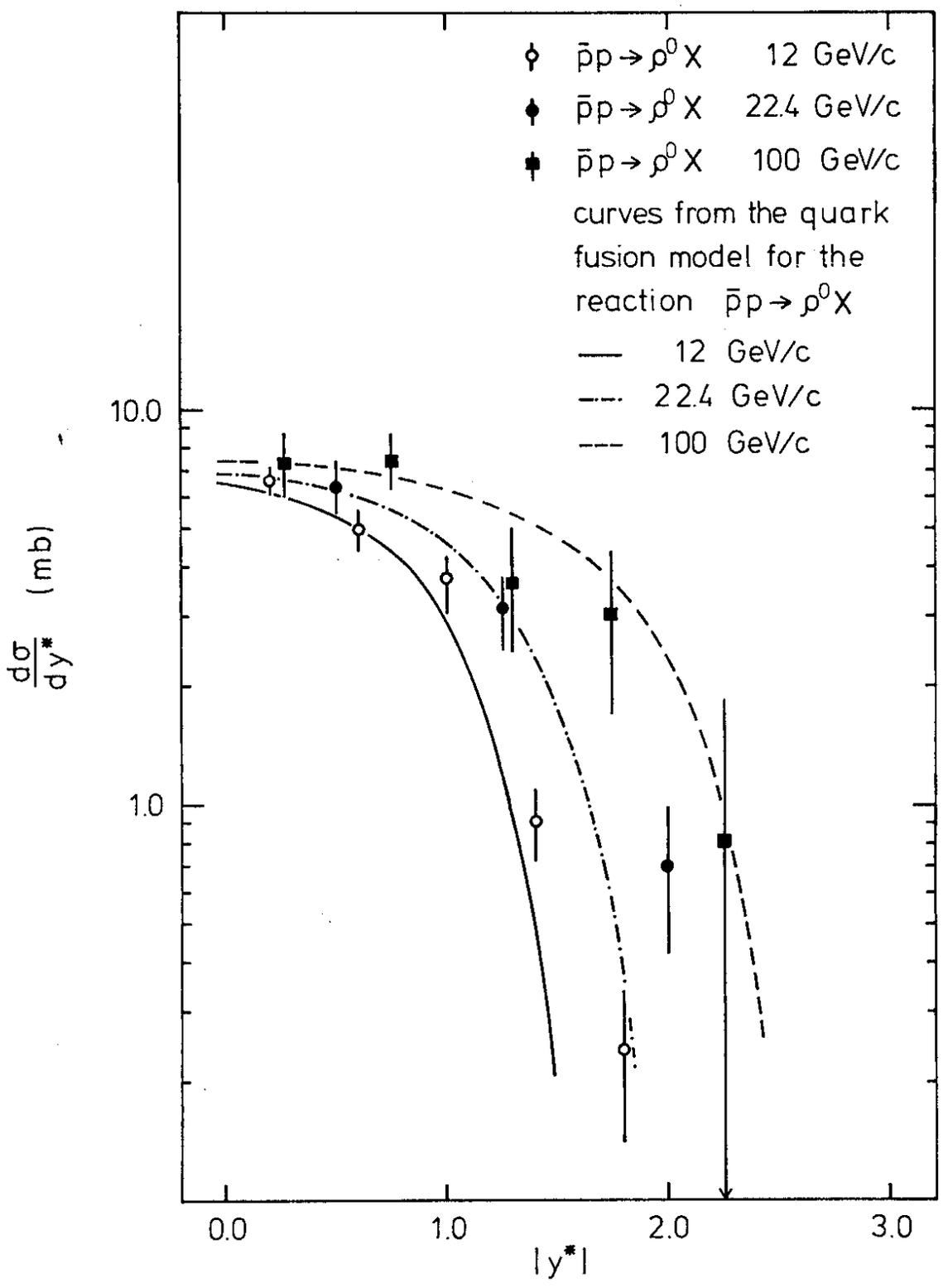
$\bar{p}p \to \rho^0 X$ 12 GeV/c
$\bar{p}p \to \rho^0 X$ 22.4 GeV/c
$\bar{p}p \to \rho^0 X$ 100 GeV/c
curves from the quark fusion model for the reaction $\bar{p}p \to \rho^0 X$
12 GeV/c
22.4 GeV/c
100 GeV/c
$\frac{d\sigma}{dy^*}$ (mb)
10.0
1.0
0.0
1.0
2.0
3.0
$|y^*|$

Fig. 14

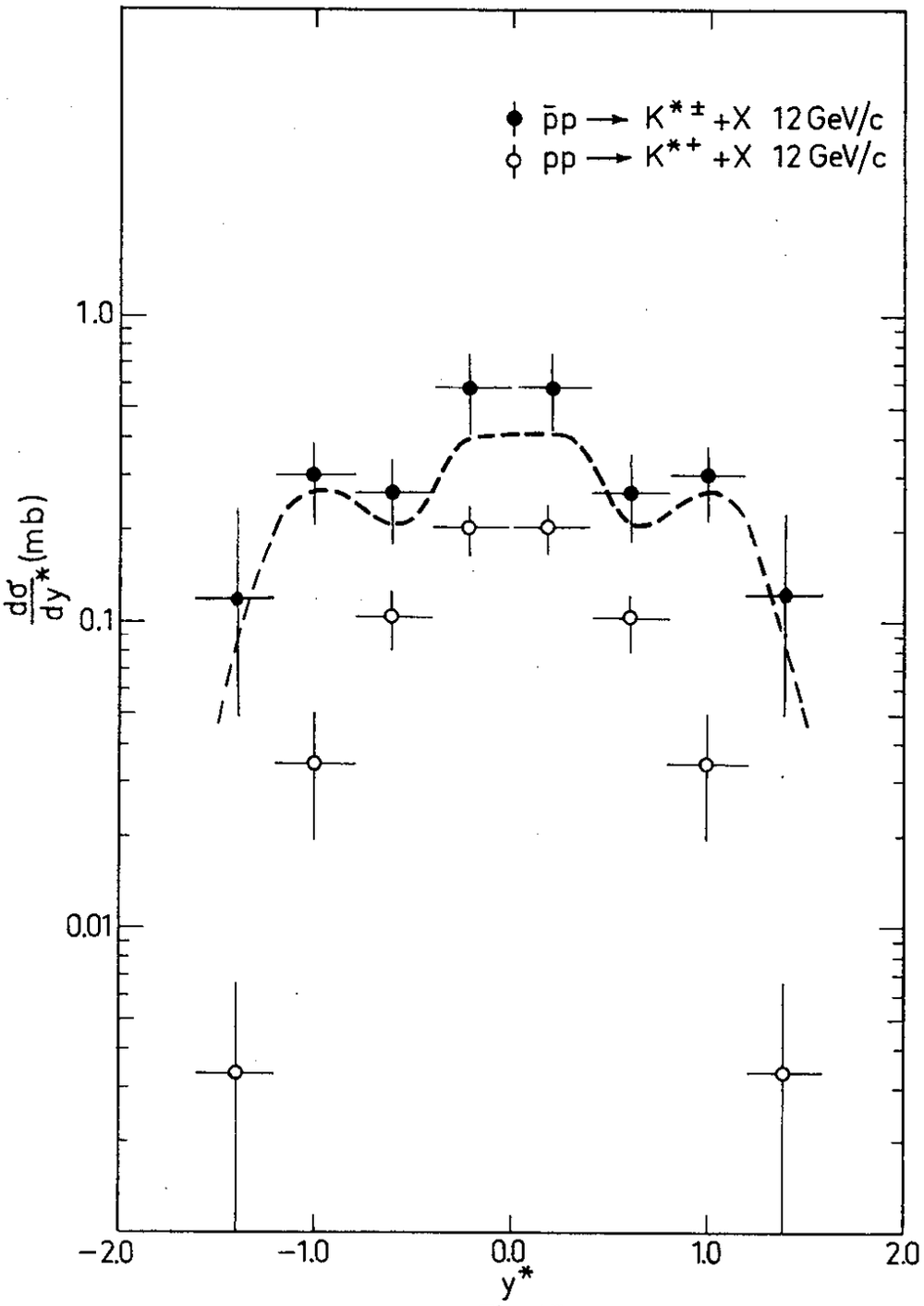
$\bar{p}p \rightarrow K^{*\pm} + X$ 12 GeV/c
$pp \rightarrow K^{*+} + X$ 12 GeV/c
1.0
0.1
0.01
$\frac{d\sigma}{dy^*}$ (mb)
−2.0
−1.0
0.0
1.0
2.0
y^*

Fig. 15

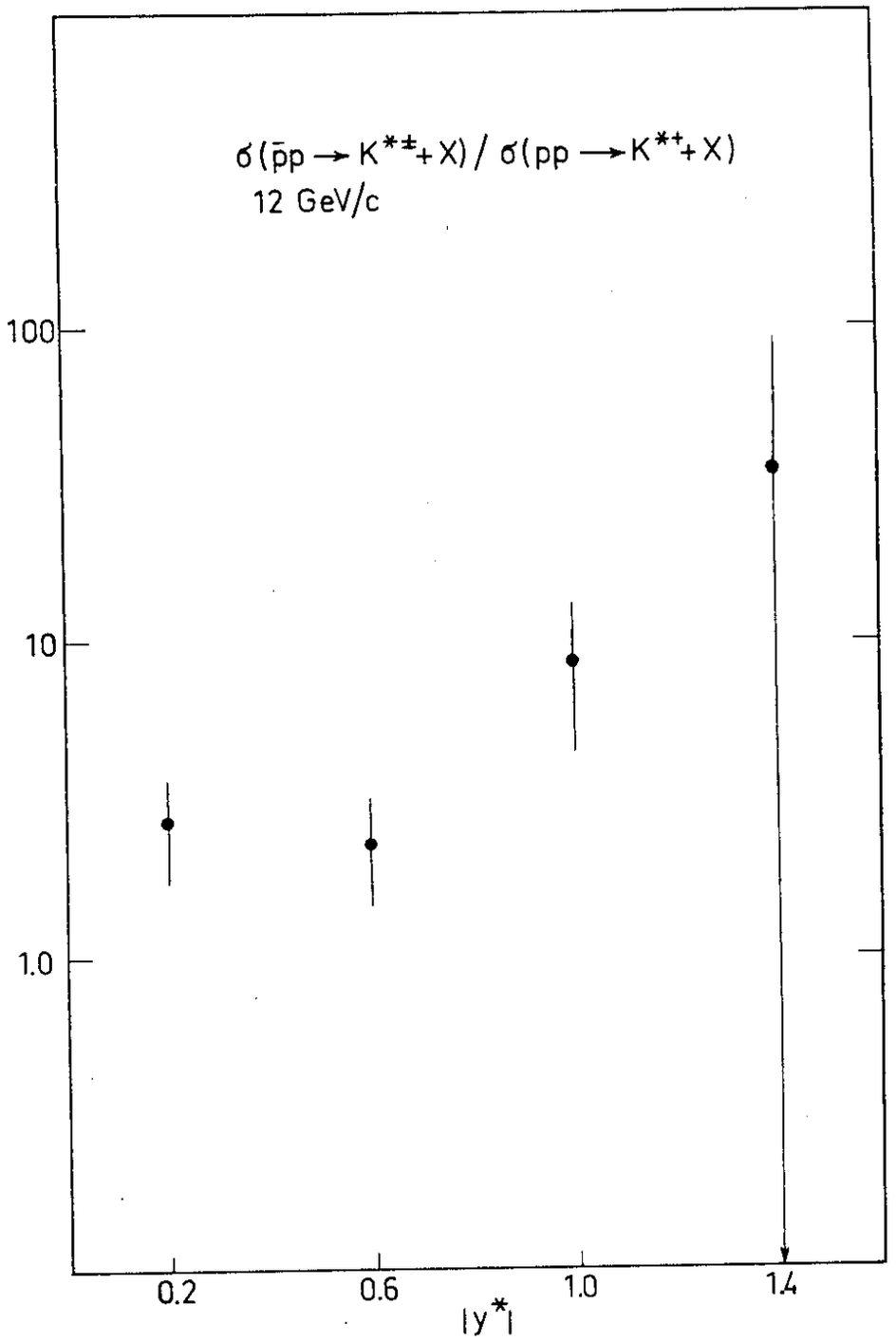

Fig. 16

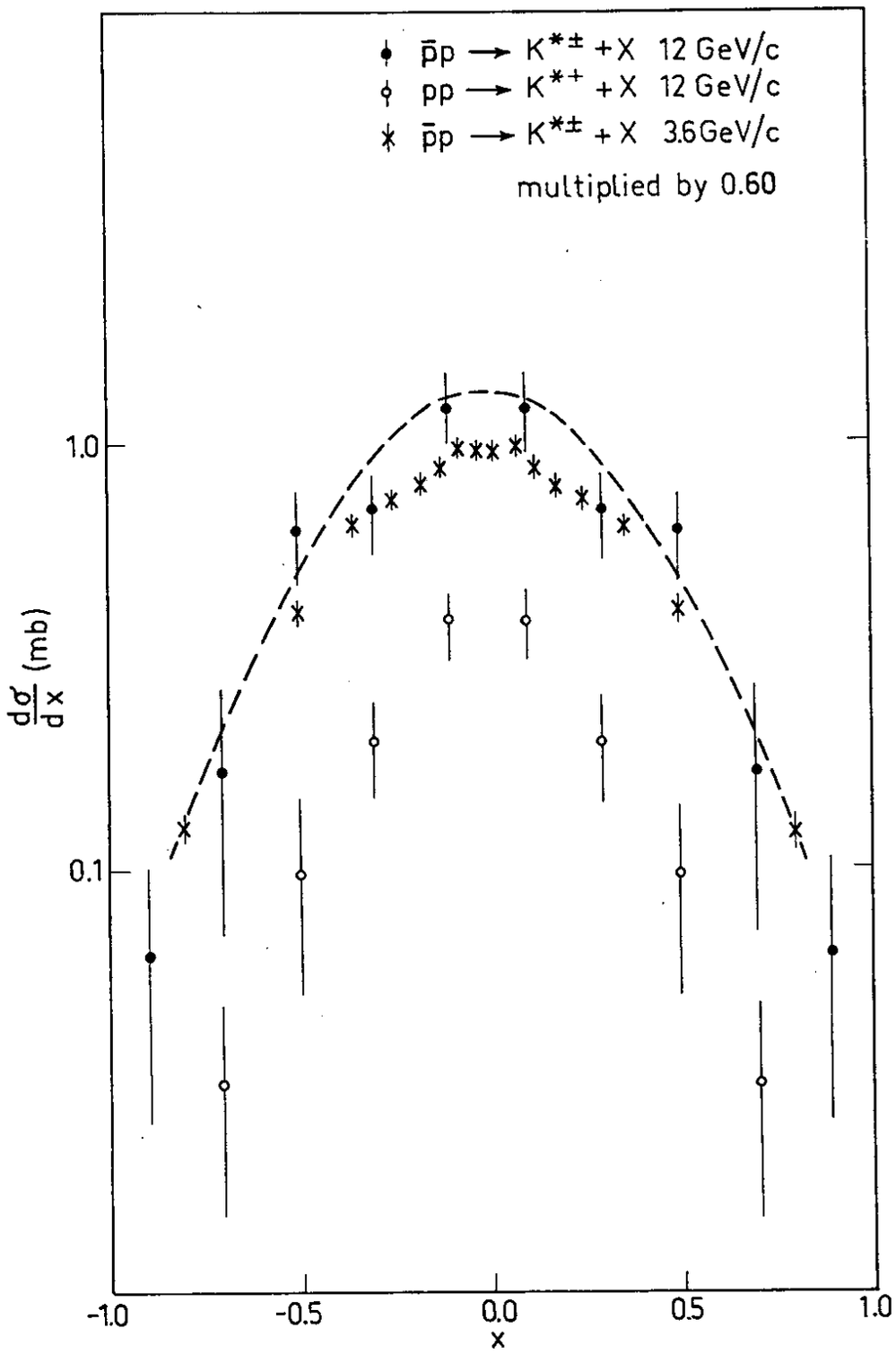
$\bar{p}p \rightarrow K^{*\pm} + X$ 12 GeV/c
$pp \rightarrow K^{*+} + X$ 12 GeV/c
$\bar{p}p \rightarrow K^{*\pm} + X$ 3.6GeV/c
multiplied by 0.60
1.0
0.1
$\frac{d\sigma}{dx}$ (mb)
-1.0
-0.5
0.0
0.5
1.0
x

Fig. 17

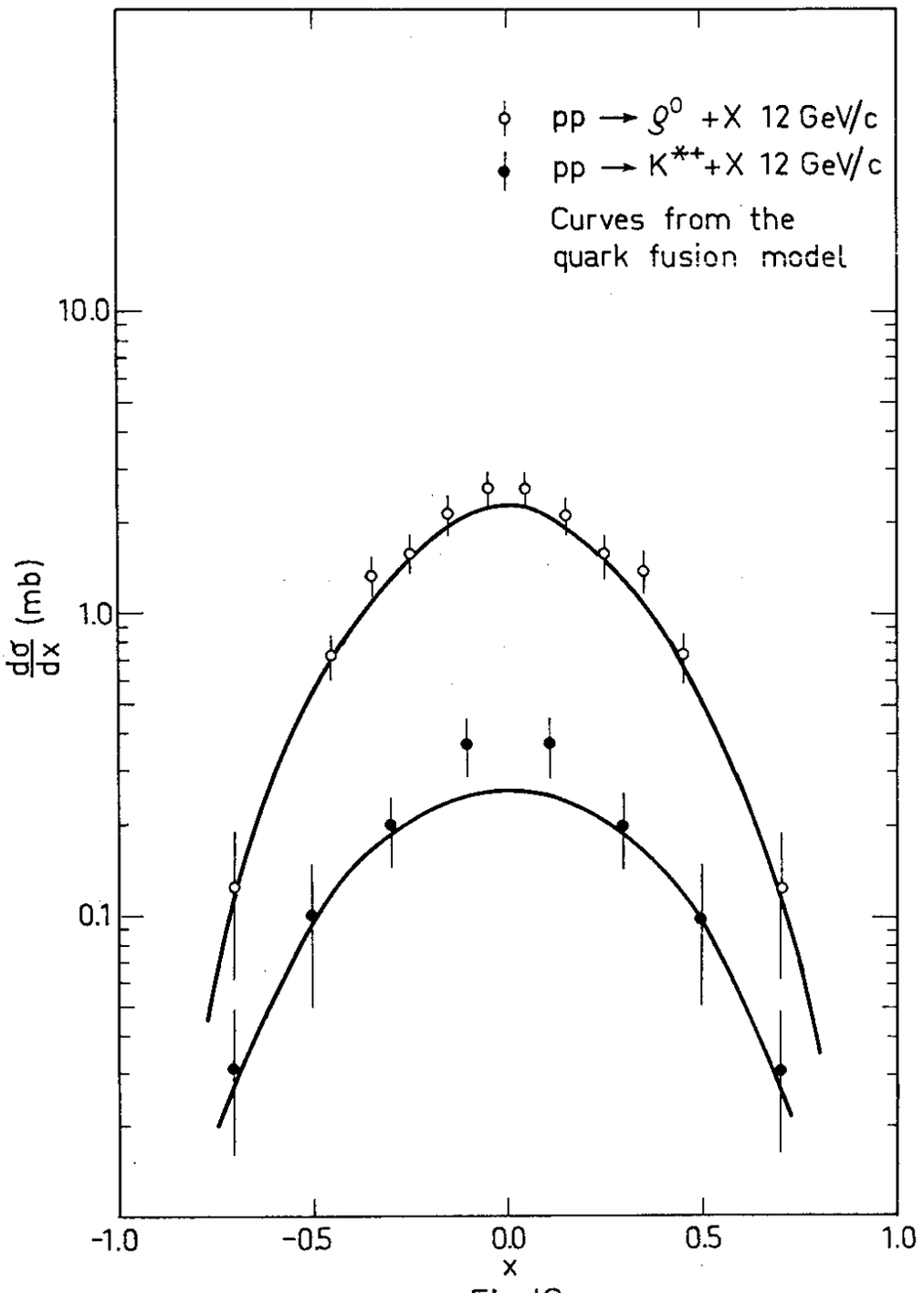
pp → ϱ⁰ +X 12 GeV/c
pp → K*⁺+X 12 GeV/c
Curves from the
quark fusion model
10.0
1.0
0.1
dσ/dx (mb)
-1.0
-0.5
0.0
0.5
1.0
x

Fig. 18

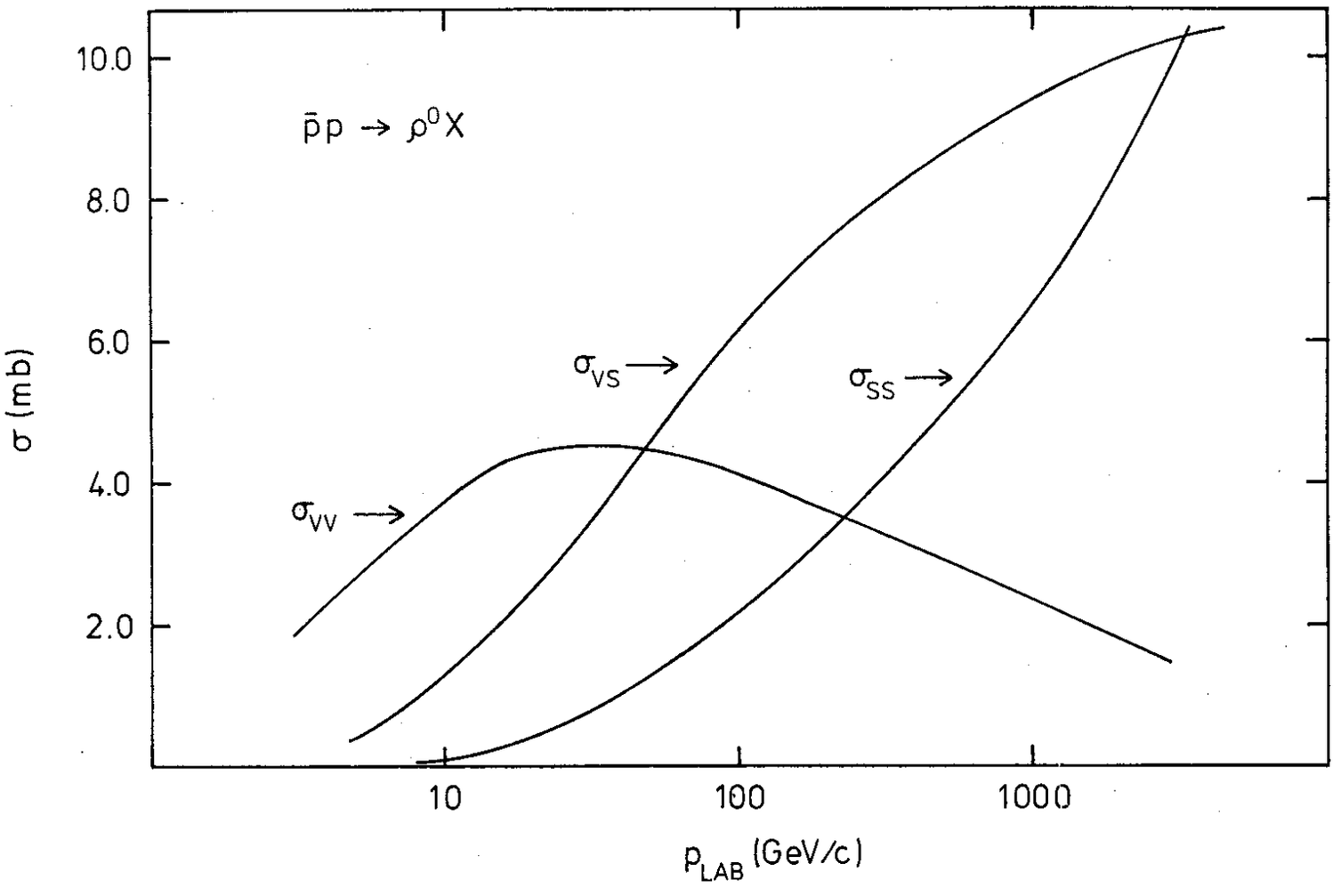

Fig. 19

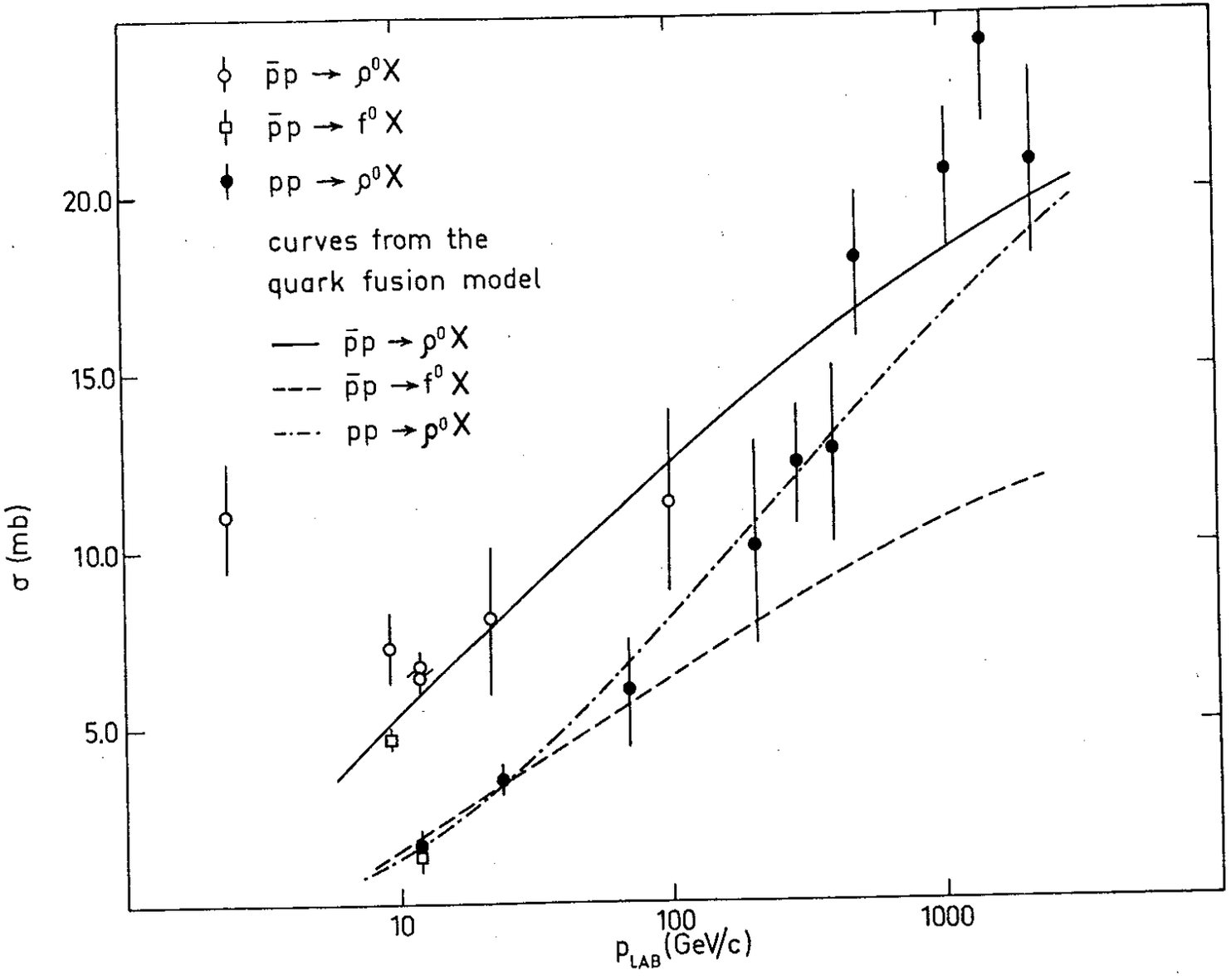
$\bar{p}p \to \rho^0 X$
$\bar{p}p \to f^0 X$
$pp \to \rho^0 X$
curves from the
quark fusion model
$\bar{p}p \to \rho^0 X$
$\bar{p}p \to f^0 X$
$pp \to \rho^0 X$
σ (mb)
20.0
15.0
10.0
5.0
10
100
1000
p_{LAB} (GeV/c)

Fig. 20

-87-